PNNL-11674
UC-2030

Ammonia Concentration Modeling Based on Retained Gas Sampler Data

G. Terrones
B. J. Palmer
J. M. Cuta

September 1997

Prepared for
the U.S. Department of Energy
under Contract DE-AC06-76RLO 1830

Pacific Northwest National Laboratory
Richland, WA 99352

DISCLAIMER

Executive Summary

The vertical ammonia concentration distributions determined by the retained gas sampler (RGS) apparatus were modeled for double-shell tanks (DSTs) AW-101, AN-103, AN-104, and AN-105 and single-shell tanks (SSTs) A-101, S-106, and U-103.[a] One-dimensional models of the vertical transport of ammonia in the tanks were used for the modeling. Transport in the non-convective settled solids and floating solids layers is assumed to occur primarily via some type of diffusion process, while transport in the convective liquid layers is incorporated into the model via mass transfer coefficients based on empirical correlations. Mass transfer between the top of the waste and the tank headspace and the effects of ventilation of the headspace are also included in the models. The resulting models contain a large number of parameters, but many of them can be determined from known properties of the waste configuration or can be estimated within reasonable bounds from data on the waste samples themselves. The models are used to extract effective diffusion coefficients for transport in the nonconvective layers based on the measured values of ammonia from the RGS apparatus.

The modeling indicates that the higher concentrations of ammonia seen in bubbles trapped inside the waste relative to the ammonia concentrations in the tank headspace can be explained by a combination of slow transport of ammonia via diffusion in the nonconvective layers and ventilation of the tank headspace by either passive or active means. Slow transport by diffusion causes a higher concentration of ammonia to build up deep within the waste until the concentration gradients between the interior and top of the waste are sufficient to allow ammonia to escape at the same rate at which it is being generated in the waste.

The results for the DSTs present a fairly consistent picture of ammonia transport. The DSTs all consist of a bottom layer of nonconvective settled solids over which lies a convective layer. A layer of floating solids lies on top of the convective liquid layer and acts as a transport barrier to the release of ammonia from the underlying liquid and settled solids layers. Values for the effective diffusion coefficient in the floating solids layer are 6–20 times that of ammonia in water, while the values in the settled solids nonconvective layer are 2 times that of ammonia in water. The only exception is Tank AN-105, where the value of the effective diffusion coefficient in the settled solids layer is 16 times that of ammonia in water. Based on the Stokes-Einstein relation, the value for the molecular diffusion coefficient for ammonia in a typical liquid waste is expected to be 20–30 times lower than the diffusion coefficient of ammonia in water, so the effective diffusion coefficients for ammonia in the DSTs appear to be high. This suggests other transport mechanisms may be present in the nonconvective layers, thus enhancing the rate of ammonia transport. Possible mechanisms are slow creeping flows within the nonconvective layers due to the presence of thermal gradients or enhanced diffusion due to bubble motion through the waste.

The SST modeling gave more variable results than the DST modeling. Unlike the DSTs, which could all be described by a single model, the SSTs required three separate models for the three tanks examined in this study. The most atypical of the SSTs was Tank A-101, which has a floating nonconvective layer on top of a convective liquid layer. The modeling of this tank

(a) Hanford waste tanks are designated with the prefix 241- plus the tank farm designation and tank number. In this report the prefix has been omitted, as it is in common usage.

suggests that the transport of ammonia through the nonconvective layer is very fast and that mechanisms other than molecular diffusion are playing a significant role. The effective diffusivity for this layer is about a factor of 5 larger than the effective diffusivities seen in any of the settled solids layers of the DSTs. Results for Tank S-106 indicate that transport through the nonconvective layer (settled solids layer for this tank) could be characterized almost completely by molecular diffusion, while results for Tank U-103 give an effective diffusivity in the nonconvective layer that is comparable to the effective diffusivity in the settled solids layers of the DSTs.

Acknowledgments

The authors are indebted to Leon Stock for clarifying the behavior of Tank A-101, to Chuck Stewart for carefully reading this manuscript and providing many useful suggestions, and to Lenna Mahoney for providing us with mass and volume fraction data for the tanks we studied.

This page is intentionally left blank.

Contents

Figures

Tables

1.0 Introduction

Ammonia is ubiquitous in the tanks storing waste at the Hanford Site. Although the concentrations vary significantly, ammonia has been found in almost all the single-shell tanks (SSTs) and double-shell tanks (DSTs) for which ammonia concentration measurements are available. The presence of ammonia in the tanks is a concern because of its toxicity (even at low concentrations) and, in extreme cases, its flammability. Because it is difficult to measure ammonia, reliable data on ammonia concentrations in the tanks have been scarce and only recently have become available. Measurements in the last year with the retained gas sampler (RGS) have begun to provide information not only on the ammonia concentration in the tanks but also on the vertical distribution of ammonia within individual tanks. This report describes efforts to fit the vertical distribution of ammonia in the RGS-sampled tanks using one-dimensional models of ammonia generation and transport. These fits are used to obtain information on ammonia transport within the tanks (for which there are no experimental data). The models assume that ammonia transport occurs by diffusion and convection. The behavior of the effective diffusion coefficients derived from the fits can be used as an indicator of the presence of transport mechanisms other than buoyancy-driven convection and molecular diffusion.

In this study, several one-dimensional mathematical models have been developed that account for convection and diffusion and provide an overall picture of ammonia transport for different configurations of tank waste. The first waste configuration investigated corresponds to DSTs in which the waste is stratified, from top to bottom, into three distinct layers: floating solids layer, convecting supernatant layer, and motionless settled solids layer. The model developed for this configuration is used to fit ammonia distributions in four DSTs: AW-101, AN-103, AN-104, and AN-105.[a] Each of these tanks has an actively ventilated dome space. The other waste configurations studied correspond to the passively ventilated SSTs, which represent three additional configurations. The waste in Tank A-101 consists of a saturated saltcake matrix floating on top of a liquid layer, while Tank S-106 has a partial floating solids layer overlying a supernatant region composed of liquid and salt slurry. Tank U-103 consists of a single layer of saltcake. In addition, the waste regions in Tanks S-106 and U-103 are highly irregular (particularly in S-106), making the location of the interface difficult to discern.

Although the models contain many parameters, including source terms for ammonia generation and mass transport across the fluid-fluid and fluid-air interfaces, most of these parameters are known or can be bounded using currently available tank monitoring data. The remaining parameters can be estimated using reasonable engineering assumptions or experimental correlations, or by applying a known steady-state solution as a boundary condition on the model calculation. A qualitative range of dissolved ammonia concentrations in the waste for the tanks listed above has recently been obtained with the RGS apparatus (Shekarriz et al. 1997). There can be a variation of a factor of 3–5 between segments in the same tank. RGS ammonia data are highly uncertain because the extraction process simply fails to measure all the ammonia in the sampler.

(a) All underground waste storage tanks at Hanford are designated with the prefix 241- followed by the tank farm designation and then the tank number. In this report, only the tank farm and tank numbers are used, the prefix is dropped.

There is also information on the ammonia concentration in the dome space for some of the tanks under consideration (Wilkins et al.).[a] All this information can be combined to fit the measured ammonia profiles and to extract effective transport coefficients for ammonia in the nonconvective layers.

In Section 2, the models used to describe the ammonia concentration distribution in DSTs and SSTs are discussed. In addition, the procedure for calculating the effective diffusion coefficients based on RGS data is also discussed. The results obtained from the solution of the various model equations are presented in Section 3, and the conclusions are summarized in Section 4. References cited are listed in Section 5, and details of the calculations and estimates of several parameters are presented in the appendixes.

(a) PNNL. 1997. TWINS Vapor Analysis Results, http://twins.pnl.gov:8001/TCD/main.html.

2.0 Mathematical Models

The models described in this section pertain to different configurations of waste stratification. The first configuration, applicable to all of the DSTs considered in this report, consists of three layers. The first of these is a buoyant, nonconvective layer floating on top of the waste. This layer is typically referred to as the crust. Beneath the crust is a convective layer consisting almost entirely of liquid, and at the bottom of the tank is a nonconvective settled solids layer sometimes referred to as the sludge. The second configuration, at present applicable only to SST Tank A-101, consists only of a nonconvective layer floating on top of a convective layer. For this configuration, there is no bottom layer of settled solids. The third configuration, applicable to SST S-106, consists of an upper convective layer overlying a nonconvective layer. The fourth configuration, applicable to SST U-103, consists of a single nonconvective layer.

The ammonia distribution is modeled by assuming that the transport of ammonia in the nonconvective layers occurs only through diffusion. The movement of ammonia in the convective layers and in the tank headspace is modeled by using mass transfer coefficients to describe the flux of ammonia from the nonconvective layers to the fluid (convective) layers. A complete set of equations describing the vertical distribution of ammonia in the tanks can be derived by coupling the transport of ammonia with the appropriate ammonia generation and destruction terms. For each layer, ammonia generation within each tank is modeled with a source term representing the thermal and radiolytic generation of ammonia within the waste. This generation rate is assumed to be constant, although in actuality it will most likely decrease gradually over time, particularly if the generation rate is tied to the level of radioactivity and the availability of a finite amount of reactants. The generation rate is also assumed to be correlated with the fraction of water (by mass) and the temperature of the waste. Because of their higher water content, liquid layers are assigned a higher generation rate than the floating and settled solids layers. The effect of ammonia degradation has also been incorporated into the model, although it is not used in our calculations.

The mass flux of ammonia between a floating solids layer and the gas in the dome or headspace is estimated from penetration theory (Cussler 1984). The mass flux between a liquid layer and the settled solids or floating solids layer is estimated from experimental correlations and by applying the analogy between heat transfer and mass transfer. Because there is convection in the dome space and in the liquid, the ammonia concentration in each of these layers is assumed to be uniform. Estimates for the various mass transfer coefficients are derived in Appendix A. Forced or natural convection in the dome space and buoyancy-driven convection in the liquid layer contribute to the turbulent mixing that leads to uniform concentrations within these regions. In addition, the dome space is assumed to be ventilated at a constant air flow rate, Q. This provides a sink term to balance generation so a steady state ammonia inventory can eventually be reached. In the absence of convection in the settled or floating solids layers (see Appendix B) it is assumed that the ammonia concentration in these layers is dominated by diffusion; thus the concentration in these layers will be nonuniform. The flux of ammonia across each interface is expressed as the product of an overall mass transfer coefficient and the concentration difference at each interface. A zero mass flux condition at the bottom of the settled solids layer is applied at the bottom of the tank.

The following is the notation for the parameters used in the model equations (for all waste configurations):

C = local ammonia concentration (in kg ammonia/m^3 waste)
z = vertical coordinate (elevation from the tank floor in m)
t = time coordinate (s).

The subscripts a, c, l, and s refer to quantities in the dome space, floating solids layer, supernatant liquid, and settled solids layer (or slurry), respectively. Parameters that can be determined from the geometry of a given tank include

L = thickness of each layer (in m)
A = cross sectional area of the tank (in m^2)
V = total headspace volume (in m^3).

Parameters that must be determined from experimental data or inferred from the physical properties of the waste or from a model of physical processes occurring in the tank include

D = the diffusion coefficient of ammonia in a layer (in m^2/s)
r = the generation rate in a given layer (in kg of ammonia/m^3 solution-sec)
k = the decay rate in a given layer (in sec^{-1})
Q = ventilation flow rate in the dome space (in m^3/s)
υ = liquid volume fraction (m^3 of liquid/m^3 of waste)
h_{ca} = the overall mass transfer coefficient of ammonia at the interface between the top of the floating solids layer and the dome space (in m/s)
h_{la} = the overall mass transfer coefficient of ammonia at the interface between the top of the supernatant and the dome space (in m/s)
h_{lc} = the mass transfer coefficient of ammonia at the interface between the bottom of the floating solids layer and the supernatant (or liquid) (in m/s)
h_{sl} = the mass transfer coefficient at the interface between the top of the settled solids layer and the supernatant liquid (in m/s).

Details of the model equations are provided in the following subsections. In most of this analysis, it is assumed that the concentration distribution of ammonia has reached a steady state (i.e., the time derivatives in the model equations below are set to zero). Time-dependent calculations with the model equations indicate that the ammonia concentration distributions in the DSTs reach 70% of their steady-state values within about 10 years. For most of the tanks, 70% is within the uncertainty in the ammonia concentrations. The effect of not being at steady state can be incorporated into the calculations in a crude way by scaling up the measured values of the ammonia concentrations. The simulations of the time-dependent model are discussed in more detail in Appendix E.

2.1 Model for DSTs

As depicted in Figure 2.1, the wastes in Tanks AW-101, AN-103, AN-104, and AN-105 contain stratified layers of settled solids and supernatant liquid capped by a floating solids layer, with gases in the dome space subjected to active ventilation.

The concentration of ammonia in the floating solids and settled solids layers is described by the one-dimensional, time-dependent diffusion equations:

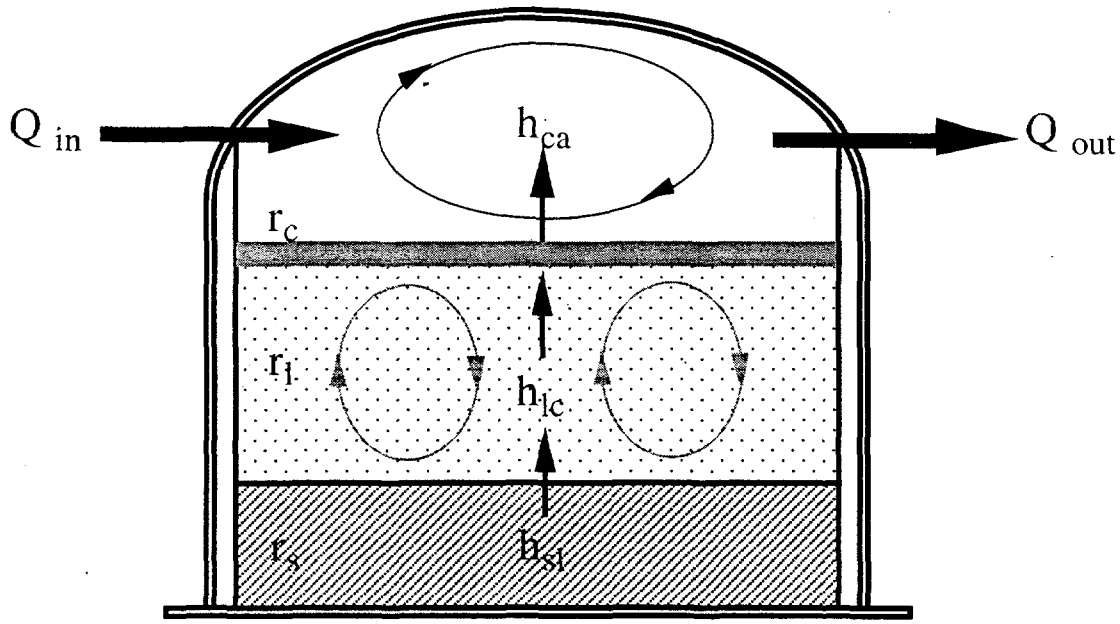

Figure 2.1. Schematic Diagram for the Settled Solids-Supernatant-Floating Solids Waste Configuration in Tanks AW-101, AN-103, AN-104, and AN-105

$$\frac{\partial C_c(z,t)}{\partial t} = D_c \frac{\partial^2 C_c(z,t)}{\partial z^2} + r_c - k_c C_c(z,t) \tag{2.1}$$

$$\frac{\partial C_s(z,t)}{\partial t} = D_s \frac{\partial^2 C_s(z,t)}{\partial z^2} + r_s - k_s C_s(z,t) \tag{2.2}$$

These equations assume that ammonia is being generated uniformly in each layer with a generation rate r and is being destroyed through a first-order process with a rate constant k.

The possibility of inserting a convective flow term of the form

$$U \frac{\partial C(z,t)}{\partial z}$$

into the equations to account for steady vertical transport of ammonia by bubble motion through the waste was considered but rejected. Here U represents the steady vertical velocity of ammonia in the waste. Although there may in fact be a steady vertical flux of bubbles through the nonconvective layers, they cannot create a net vertical current. The liquid fraction in the nonconvective layers is expected to be relatively constant, and there is no net flux of liquid at the surface of any of these layers. Therefore, conservation of mass requires that any upward microcurrents of liquid in the nonconvective waste caused by bubble motion must be balanced by an equal flux of downward microcurrents. The disordered nature of the channels in the waste implies that these microcurrents

are only significant on a very small length scale, probably not much more than a factor of 10 larger than a typical grain size. These microcurrents might manifest themselves as enhanced diffusion of ammonia but would not be present as a steady convective flux. An exception to this argument is the possibility that ammonia is being carried up through waste inside bubbles. Unlike what occurs in the liquid fraction of the waste, insoluble gas generated throughout the tank does result in a net flux of bubbles through the different tank layers. However, the amount of ammonia being released into the tank headspace via this mechanism can be estimated using the RGS results for the relative amounts of retained gas in the tanks and measurements of the hydrogen and ammonia concentrations in the tank headspace. Estimates of the amount of ammonia released by convective transport in bubbles are given for four of the tanks described in this report in Appendix C and indicate that the maximum amount of ammonia released by this mechanism is less than 10%.

The concentration of ammonia in the supernatant liquid layer is given by the expression

$$\frac{d\,C_l(t)}{d\,t} = \frac{1}{L_l}\left\{ h_{sl}\left[\frac{C_s(L_s,t)}{\upsilon_s} - C_l(t)\right] - h_{lc}\left[C_l(t) - \frac{C_c(L_s+L_l,t)}{\upsilon_c}\right]\right\} + r_l - k_l\,C_l(t) \quad (2.3)$$

This equation assumes that ammonia entering and leaving the convective layer from the floating solids and settled solids layers can be described by mass transfer coefficients. Ammonia can also be generated and destroyed locally within the supernatant layer via processes similar to those in the floating solids and settled solids layers. The appearance of the volume fractions in the denominator in this equation is to reference concentration only to the liquid. There must be a difference between the concentration in the interstitial liquid in the floating solids or settled solids layers in the tank and the supernatant liquid before there is any mass flux.

The equation for the concentration of ammonia in the tank headspace is similar to the equation for the supernatant liquid:

$$\frac{d\,C_a(t)}{d\,t} = \frac{A\,h_{ca}}{V}\left[\frac{C_c(L_s+L_l+L_c,t)}{\upsilon_c} - C_a(t)\right] - \frac{Q\,C_a(t)}{V} \quad (2.4)$$

The flux of mass into the tank headspace due to evaporation of ammonia from the floating solids layer is described by the mass transfer coefficient, h_{ca}, and the loss of ammonia from the headspace is due to the tank ventilation. Unlike the waste layers of the tank, there is no local generation or destruction of ammonia in the headspace.

The remaining equations describing the ammonia concentration in the tank are all obtained by requiring that the mass flux be conserved across the different tank layers. At the bottom of the tank, the zero flux boundary condition

$$0 = -D_s \left.\frac{\partial\,C_s(z,t)}{\partial\,z}\right|_{z=0} \quad (2.5)$$

is applied to the concentration. The boundary conditions for the remaining three interfaces all follow from the requirement that the mass flux due to diffusion equal the mass flux due to the mass transfer relations. This yields

$$\left\{h_{ca}\left[\frac{C_c(z,t)}{\upsilon_c}-C_a(t)\right]=-D_c\,\frac{\partial C_c(z,t)}{\partial z}\right\}\Bigg|_{z=L_a+L_l+L_s} \tag{2.6}$$

$$\left\{h_{lc}\left[C_l(t)-\frac{C_c(z,t)}{\upsilon_c}\right]=-D_c\,\frac{\partial C_c(z,t)}{\partial z}\right\}\Bigg|_{z=L_l+L_s} \tag{2.7}$$

$$\left\{h_{sl}\left[\frac{C_s(z,t)}{\upsilon_s}-C_l(t)\right]=-D_s\,\frac{\partial C_s(z,t)}{\partial z}\right\}\Bigg|_{z=L_s} \tag{2.8}$$

The mass transfer coefficients h_{ca}, h_{lc}, and h_{sl} appearing in equations 2.6–2.8 can be estimated from the waste properties (see Appendix A). The coefficients for h_{lc} and h_{sl} are obtained from engineering correlations developed for heat transfer between two surfaces and exploit the analogy between heat and mass transfer; the coefficient h_{ca} is obtained from a simple analytic theory of the transfer between the floating solids layer and the gas in the tank headspace.

2.2 Models for SSTs

Unlike the DSTs, the waste configuration is not uniform for the SSTs. In some instances, there is no clear-cut distinction between a liquid layer and slurry layer or the interfaces between a fluid saturated and a partially saturated solid-liquid-gas matrix. In addition, there is clear evidence that the waste configuration varies markedly in the radial direction. In the SSTs there are far fewer RGS ammonia concentration data points per riser than in the DSTs.

2.2.1 Tank A-101

In Tank A-101, the waste consists of a saturated saltcake matrix that overlies a convective liquid layer (see Figure 2.2). Applying the same set of assumptions for global transport of ammonia and the conservation of mass equation that were used to develop the equations for the DSTs to the configuration shown in Figure 2.2 leads to the following one-dimensional, time-dependent diffusion equations and boundary conditions to describe the ammonia concentration distribution:

$$\frac{dC_a(t)}{dt}=\frac{A\,h_{ca}}{V}\left[\frac{C_c(L_l+L_c,t)}{\upsilon_c}-C_a(t)\right]-\frac{QC_a(t)}{V} \tag{2.9}$$

$$\frac{\partial C_c(z,t)}{\partial t}=D_c\,\frac{\partial^2 C_c(z,t)}{\partial z^2}+r_c-k_c\,C_c(z,t) \tag{2.10}$$

$$\left\{h_{ca}\left[\frac{C_c(z,t)}{\upsilon_c}-C_a(t)\right]=-D_c\,\frac{\partial C_c(z,t)}{\partial z}\right\}\Bigg|_{z=L_l+L_s} \tag{2.11}$$

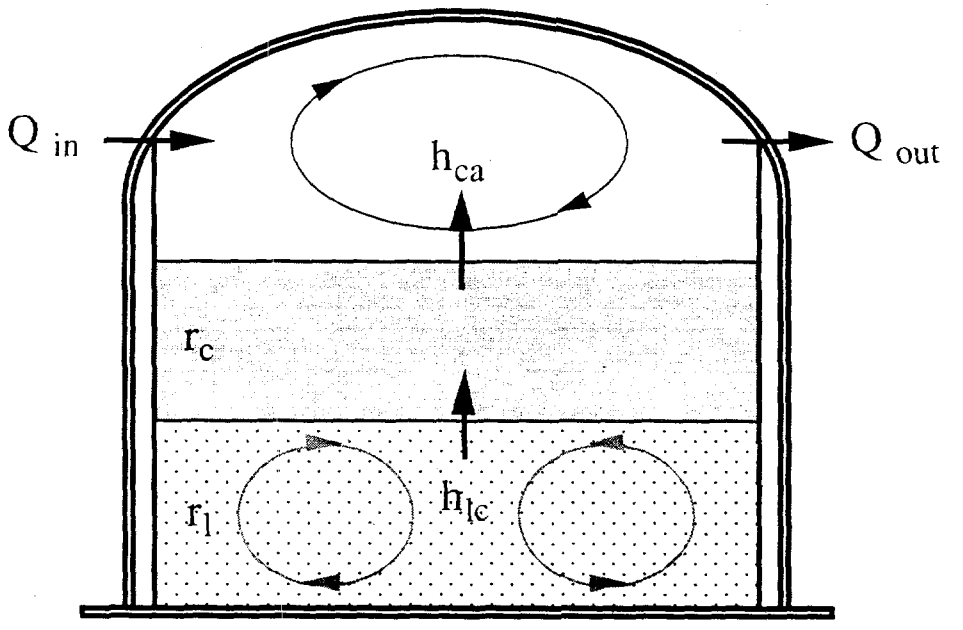

Figure 2.2. Schematic Diagram of the Liquid-Floating Solids Waste Configuration in Tank A-101

$$C_l(t) = \frac{C_c(L_l, t)}{\upsilon_c} \tag{2.12}$$

$$\frac{dC_l(t)}{dt} = r_l + \frac{D_c}{L_l}\frac{\partial C_c(z,t)}{\partial z}\bigg|_{z=L_l} - k_l C_l(t) \tag{2.13}$$

Eq. (2.9) models the flux of ammonia into and out of the dome space; Eq. (2.10) models the diffusion, generation, and destruction of ammonia in the floating nonconvective layer; Eq. (2.11) is the boundary condition between the nonconvective layer and dome space and essentially requires that the flux of ammonia out of the nonconvective layer equal the flux of ammonia into the dome space; Eq. (2.12) is the boundary condition between the nonconvective layer and the liquid layer that requires continuity of the concentration at the interface; and Eq. (2.13) is the mass balance equation between internal generation of ammonia and mass flux out of the liquid layer. These equations simply assume that the ammonia concentration in the liquid fraction is equal across the interface between the nonconvective and liquid layers.

2.2.2 Tank S-106

Information on the nature of the waste distribution obtained from three risers in Tank S-106 indicates a three-dimensional configuration that varies substantially from riser to riser.[(a)] There is a thick floating solids layer on the periphery of the tank, while at the center there is none. In addition, there are no horizontal interfaces between the various identified regions such as liquid, salt slurry, wet salt, and moist salt (the terminology used to describe gas-solid-liquid

(a) Mousel A. 1997. S-106 PMCS Core Profile. File S106.CRD, Los Alamos Technical Associates, Richland, Washington.

clusters from core samples is merely qualitative). For modeling purposes, it is assumed that there are two layers whose interface is obtained from the average levels of supernatant (liquid and salt slurry) in risers 7 and 8 (which are near the center of the tank at the same radial distance but 90° apart). Because the upper layer is a mixture of liquid and solids, the ammonia concentration in this layer must be scaled by the liquid volume fraction υ_l. The lower layer is assumed to include wet salt, moist salt, and salt slurry. A schematic of the simplified stratification of waste in S-106 used for modeling is shown in Figure 2.3.

The model equations to be used in this case are

$$\frac{dC_a(t)}{dt} = \frac{A h_{la}}{V}\left[\frac{C_l(t)}{\upsilon_l} - C_a(t)\right] - \frac{Q C_a(t)}{V} \tag{2.14}$$

$$\frac{dC_l(t)}{dt} = r_l - \frac{D_s}{L_l}\frac{\partial C_s(L_s,t)}{\partial z} - \frac{h_{la}}{L_l}\left[\frac{C_l(t)}{\upsilon_l} - C_a(t)\right] - k_l C_l(t) \tag{2.15}$$

$$\frac{\partial C_s(z,t)}{\partial t} = D_s \frac{\partial^2 C_s(z,t)}{\partial z^2} + r_s - k_s C_s(z,t) \tag{2.16}$$

$$\frac{C_l(t)}{\upsilon_l} = \frac{C_s(L_s,t)}{\upsilon_s} \tag{2.17}$$

$$0 = -D_s \frac{\partial C_s(z,t)}{\partial z}\bigg|_{z=0} \tag{2.18}$$

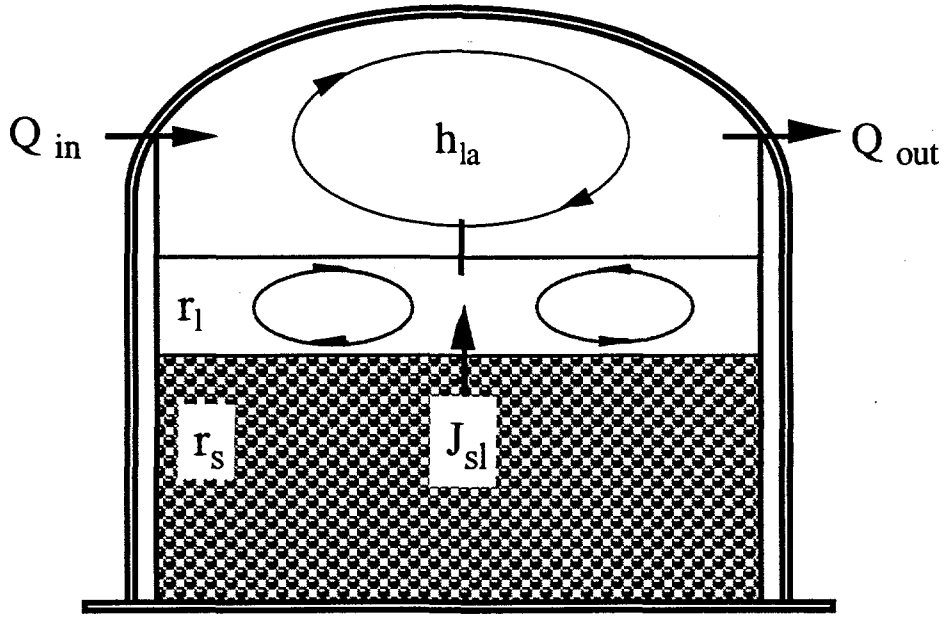

Figure 2.3. Schematic Diagram for the Liquid-Slurry Waste Configuration in Tank S-106

Eq. (2.14) models the flux of ammonia into and out of the dome space; Eq. (2.15) is the mass balance equation between internal generation of ammonia and mass flux into and out of the supernatant (drainable liquid and solids); Eq. (2.16) models the diffusion, generation, and destruction of ammonia in the slurry layer (salt slurry, wet salt, and moist salt); Eq. (2.17) is the boundary condition between the supernatant and the slurry layer that requires continuity of the concentration at the interface; and Eq. (2.18) is the zero flux condition for ammonia at the bottom of the tank. As in the model for Tank A-101, it is assumed that the ammonia concentration in the liquid fraction is equal across the interface between the slurry and supernatant layers. Unlike the model for DSTs, the incoming mass flux from the slurry to the supernatant layer is not modeled with an overall mass transfer coefficient.

2.2.3 Tank U-103

Core sample information for Tank U-103[a] indicates the presence of two layers, a bottom layer composed of moist salt and a top layer consisting of a liquid-salt slurry. A partial floating solids layer has been observed, but the area covered by the floating solids layer is smaller than that of the liquid-salt slurry (Brevick et al. 1994). It is assumed that the ammonia transfer occurs directly between the liquid-salt slurry and the gas in the dome space. Because there is no evidence of a convective layer, the two layers are treated as a single nonconvective layer and the model equations for Tank U-103 are based on diffusion within a single layer. A schematic of the simplified stratification of waste in U-103 used for modeling is shown in Figure 2.4.

The model equations to be used in this case are

$$\frac{dC_a(t)}{dt} = \frac{A\,h_{sa}}{V}\left[\frac{C_s(L_s,t)}{\upsilon_s} - C_a(t)\right] - \frac{Q\,C_a(t)}{V} \tag{2.19}$$

$$\frac{\partial C_s(z,t)}{\partial t} = D_s\,\frac{\partial^2 C_s(z,t)}{\partial z^2} + r_s - k_s\,C_s(z,t) \tag{2.20}$$

$$\left\{h_{sa}\left[\frac{C_s(z,t)}{\upsilon_s} - C_a(t)\right] = -D_s\,\frac{\partial C_s(z,t)}{\partial z}\right\}\Bigg|_{z=L_s} \tag{2.21}$$

$$0 = -D_s\,\frac{\partial C_s(z,t)}{\partial z}\Bigg|_{z=0} \tag{2.22}$$

Eq. (2.19) models the flux of ammonia into and out of the dome space; Eq. (2.20) models the diffusion, generation, and destruction of ammonia in the nonconvective layer; Eq. (2.21) is the boundary condition between the nonconvective layer and dome space and essentially requires that the flux of ammonia out of the nonconvective layer equals the flux of ammonia into the dome space; and Eq. (2.22) is the zero flux condition for ammonia at the bottom of the tank.

(a) Mousel A. 1997. U-103 PMCS Core Profile. File U103.CRD. Los Alamos Technical Associates, Richland, Washington.

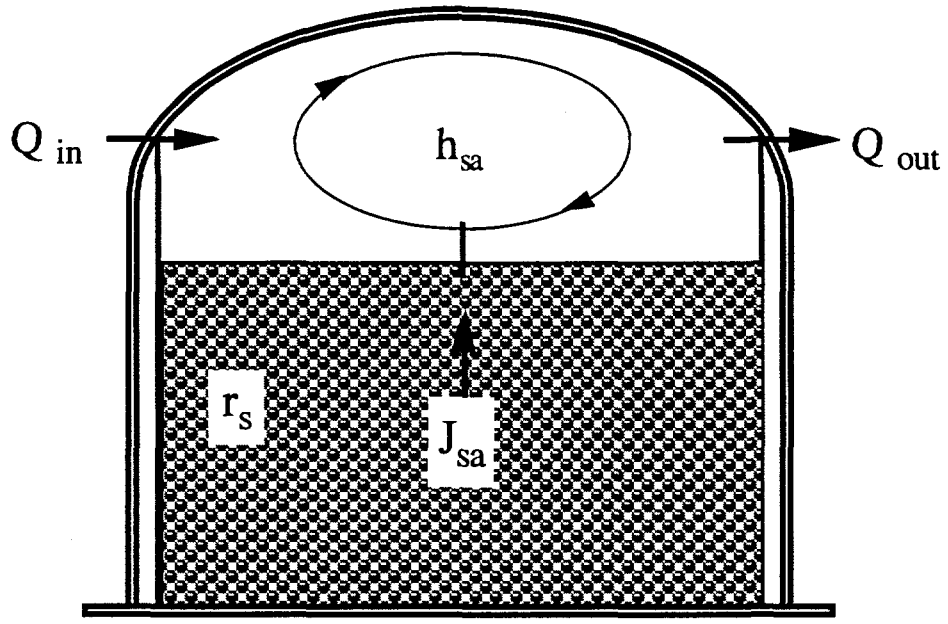

Figure 2.4. Schematic Diagram for the Nonconvective Liquid-Slurry Waste Configuration in Tank U-103

2.3 Model Parameters

Based on measurements of the conditions in DSTs and SSTs (Stewart et al. 1996; Hodgson et al. 1996; Shekarriz et al. 1997; Meyer et al. 1997), most of the input parameters required by the one-dimensional models for ammonia transport can be calculated (see Appendix A). Table 2.1 shows the thickness of each layer (in all cases the cross-sectional area of each tank is 410.43 m^2). Table 2.2 shows the ventilation flow rates measured in DSTs [(a)] and SSTs (Huckaby et al. 1997) with an assumed value for S-106 [(b)] (the dome space in SSTs is passively ventilated, which means the ventilation flow rate is about 1–2 orders of magnitude smaller than that in DSTs), the mass water fractions, ω_x, and liquid volume fractions υ_x (see Appendix A).

For Tank A-101, the liquid volume fraction in the floating solids layer, υ_c, was calculated following a procedure that does not involve the waste densities.[(c)] For the remaining tanks considered here, sufficient information was available to calculate the liquid volume fractions based on density data. It is assumed for A-101 that all of the ammonia is in the liquid portion of the waste and the water in the waste mixture is saturated with salts. The transformation of the ammonia concentrations (Shekarriz et al. 1997) from micromoles per liter of waste (MPLW) into micromoles of ammonia per liter of liquid (MPLL) is simply MPLL = MPLW/υ_c.

The water contents for the segments of the cores adjacent to the RGS segments have approximately 35% water by weight (Field et al. 1997), so 1000 grams of gas-free waste contain 350 grams of water (in the liquid state occupies 350 mL at 25°C) and 650 grams of inorganic

(a) Personal communication, DJ Minteer (DESH) to G Terrones (PNNL), April 25, 1997.
(b) Personal communication, JL Huckaby (PNNL) to G Terrones (PNNL), September 8, 1997.
(c) Personal communication, LM Stock (DES) to G Terrones (PNNL), September 9. 1997.

Table 2.1. Physical Dimensions

	AW-101	AN-103	AN-104	AN-105	A-101	S-106	U-103
L_c (m)	0.64±0.15	0.92±0.2	0.4±0.1	0.3±0.1	4.25±0.24	-	-
L_l (m)	6.93±0.19	4.13±0.16	5.24±0.1	5.59±0.11	4.97±0.24	1.00±0.2	-
L_s (m)	2.83±0.22	3.79±0.9	4.15±0.9	4.52±0.11	-	3.56±0.7	4.22±0.48
V (m^3)	1065	1717	1321	1024	1224	2197	1448

Table 2.2. Flow Rates, Water, and Liquid Fractions

	AW-101	AN-103	AN-104	AN-105	A-101	S-106	U-103
Q (m^3/s)	0.059±.02	0.0472±.01	0.0472±.01	0.0472±.01	$4.75x10^{-3}$	$9.44x10^{-4}$	$1.28x10^{-3}$
ω_c	0.34±.05	0.17±.01	0.35±.07	0.33±.10	0.36±.02	-	-
ω_l	0.44±.02	0.44±.03	0.53±.03	0.51±.01	0.47±.01	0.53±.01	0.51±.003
ω_s	0.32±.05	0.15±.01	0.33±.07	0.32±.10	-	0.18±.006	0.20±.005
υ_c	0.63±.10	0.37±.02	0.65±.13	0.63±0.20	0.63±.02	-	-
υ_s	0.71±.11	0.38±.02	0.68±.14	0.69±0.22	-	0.38±.006	0.41±0.01
υ_l	0.99±.004	0.99±.006	0.99±.005	0.99±.006	0.99±.007	0.85±.003	-

substances distributed among the liquids and solids. In addition, the measured density of the gas-free waste is 1700 g/L at 25°C (Field et al. 1997), so 1000 g of waste occupies 588 mL.

As a first approximation, υ_c can be calculated on the basis of the water content of the waste in the nonconvective layer. In this situation the fraction of liquid is approximately 0.6. As a second approximation, υ_c can be calculated on the basis of the more realistic situation in which the water in the waste mixture is saturated with salts. The high concentrations of dissolved salts will cause the volume of the aqueous salt solution to expand beyond 350 mL. Elementary considerations suggest the dissolved salt will cause the fraction of the liquid to increase by about 10%. The total volume of 1000 g of waste, which is determined by the density, will not change. This yields a liquid fraction of approximately 0.65.

Table 2.3 shows ammonia concentrations in the various regions in each tank (in units of μmol/L waste). The concentrations marked with an asterisk were calculated using an earlier version of the RGS data reduction procedure that may have substantially underestimated the ammonia concentrations. A more sophisticated data reduction procedure was applied to Tanks S-106 and U-103 and is believed to give more reliable values for the ammonia concentrations. Ammonia concentration measurements in the dome space were reported for several tanks by Wilkins et al. (1997). For most of the Hanford tanks, information on ammonia dome space concentration can be found on the internet under Vapor Analysis Results.[a] For the convective and nonconvective

(a) http://twins.pnl.gov:8001/TCD/main.html.

Table 2.3. Ammonia Concentrations in μmol/L Waste

	AW-101	AN-103	AN-104	AN-105	A-101	S-106	U-103
C_a	0.495	< 0.708	< 0.708	1.062	53.053	2.583	52.063
C_c	-	1,260*	-	-	6,212*	-	-
C_l	960*	1,980*	1,100*	920*	16,352*	1,000 ± 50%	-
C_s	2,329*	2,965*	2,406*	1,565*	-	3,067 ± 50%	28,450 ± 50%

* These quantities could be up to one-third of the actual values.

layers, only qualitative estimates on the ammonia concentration are shown in Table 2.3 (from RGS data) (Shekarriz et al. 1997)[a,b]. To back-calculate the effective diffusion coefficients in the layers in which molecular diffusion dominates, a spatial average for the RGS ammonia concentration in the floating solids layer and settled solids layer/slurry (whenever data were available) was used as input in the models.

2.4 Modeling Ammonia Profiles

To model the ammonia distribution, it was postulated that the observed ammonia concentration in the tanks was produced by generation rates in each layer that were proportional to the water mass fraction and some function of the average temperature in each layer in the following form:

$$r_x = K \omega_x F(T)$$

where K is a proportionality constant, ω_x is the water fraction in the layer, and F(T) is a function representing the temperature dependence of ammonia generation. However, based on the experimental data of Bryan et al. (1996) for Tank SY-103, the changes in the generation rate between the different layers within a given tank due to temperature variations amount to less than 6% for the tanks studied here, and the function F(T) can be considered more or less constant for a given tank. It can therefore be absorbed into the proportionality constant K. It is also assumed that the degradation of ammonia via first-order processes was negligible, in accord with the findings of Bryan and Pederson (1996). Lilga et al. (1996) recently proposed that ammonia is degraded at a significant rate by zero-order processes, but this can be absorbed into the generation rate. A significant zero-order destruction rate may have an effect on the assumption that the generation rate is proportional to the water mass fraction in the waste. The assumption that the specific generation rate in each layer is proportional to the mass fraction of water in the layer reduces the three independent generation rates to a single proportionality constant. If the water fractions are known for all the layers, then the proportionality constant can be found by requiring that the total ammonia generation rate in the tank waste match the amount of ammonia leaving the tank by ventilation of the dome

(a) Mahoney LA, ZI Antoniak, JM Bates, and A Shekarriz. 1997. *Preliminary Retained Gas Sampler Measurement Results for Hanford Waste Tank 241-S-106.* TWSFG97.47, PNNL, Richland, Washington.
(b) Mahoney LA, ZI Antoniak, JM Bates, and A Shekarriz. 1997. *Preliminary Retained Gas Sampler Measurement Results for Hanford Waste Tank 241-U-103.* TWSFG97.40, PNNL, Richland, Washington.

space assuming the waste has reached steady state. The amount of ammonia leaving the tank by ventilation can, in turn, be calculated from the measured headspace concentration of ammonia and the tank ventilation rate. The only remaining adjustable parameters for the DSTs are the effective diffusion coefficients of ammonia in the upper and lower nonconvective layers. These two unknowns can be solved by requiring that the equations for the ammonia distribution reproduce the average of the measured concentrations of ammonia in the settled solids and supernatant layers. This provides two conditions that fix the two unknowns. For the SSTs, each waste configuration is different; thus there are several sets of adjustable parameters depending on whether there is convection in the liquid layer and on the type of boundary condition (mass flux or concentration continuity) imposed between the liquid and the floating solids layer (or slurry, or settled solids layer). Whatever the case, the diffusivities of the one or two nonconvective layers are adjustable parameters for which a solution is sought.

Because estimates on the ammonia concentration profile are known experimentally from measurements at a few locations, the task of determining some of the model parameters in the model equations can be treated as an inverse problem (i.e., certain input parameters can be back-calculated from experimental data). For the DSTs, all parameters except the effective diffusivities in the settled solids and floating solids layers are known (within a range of values). These parameters are then determined by matching the average measured ammonia concentration in the settled solids and supernatant layers. The most poorly determined parameters in the model for the DSTs are probably the mass transfer coefficients between the liquid and the nonconvecting layers. However, parameter sensitivity studies with the model for the DSTs have shown that in most cases the ammonia concentrations are only weakly dependent on the mass transfer coefficients, h_{lc} and h_{sl}. For the SSTs, the calculation procedure is basically the same as that for the DSTs except that there might not always be two diffusivities to determine, rather, a diffusivity and another parameter such as a mass transfer coefficient.

As discussed above, the reported RGS ammonia concentration data are highly uncertain (Shekarriz et al. 1997). The RGS concentrations (for the DSTs and SST Tank A-101) may be 3 to 5 times lower than the actual value. The tanks may also not be at steady state, which would imply that the ammonia concentrations used in the calculations are most likely too low. To account for this variability in the data, a concentration correction factor, f, is introduced ($1 < f < 5$) to scale the measured concentrations. Values of the concentration inside the tank waste used in the calculations are scaled by

$$C_x(z) = f\, C_{RGSx}(z)$$

The adjustable parameters calculated from the concentrations are implicitly functions of the scale factor, f. Values for the transport coefficients obtained using $f = 1$ assume that the reported RGS values for the concentration are accurate. Values obtained using $f = 3$ assume that the RGS values only represent one-third of the actual concentration.

Solutions are found for the transport coefficients by matching the average of the experimental concentration data to the spatial average of the analytically obtained solution for the concentration from the model equations. The spatial average of the concentration for each waste layer can be obtained from the analytical solutions of the model by evaluating the integrals:

$$\overline{C}_x = \frac{1}{L_x} \int C_x(z)\, dz$$

For DSTs the average concentration in the settled solids and supernatant layers are used to fix the effective diffusivities in the floating solids and settled solids layers (except for AN-103, there are no ammonia data for the floating solids layer). For SSTs, the average concentration in the nonconvective layer was used to fix the effective diffusivity in the nonconvective layer. The calculated ammonia concentration profiles and the dependence of the adjustable parameters as a function of the concentration correction factor for the various tanks are presented below to provide some insight on the general trend in which ammonia is distributed and to ascertain whether transport mechanisms other than convection and diffusion take place.

To take into account the uncertainty in the many parameters used as input, several Monte Carlo calculations were performed to determine the distribution of diffusivities in the nonconvective layers. These calculations were based on the solutions for the diffusivities derived from the steady-state model equations. The averages and standard deviations were also calculated.

3.0 Results

Results for Tanks AW-101, AN-103, AN-104, AN-105, A-101, S-106, and U-103 are summarized in this section. Ammonia generation rates for each of the tank layers were calculated from the headspace ammonia concentrations as described in Section 2. The generation rates were combined with the ammonia concentrations measured with the RGS apparatus as were estimates of other tank and waste properties to calculate the effective diffusivities for the nonconvective layers in each of the tanks. These diffusivities are important for determining how much ammonia can be expected to build up in the tanks and can also provide an indication of how fast concentration fluctuations of other components can be expected to relax.

The broad range in uncertainty of some of the parameters used in these calculations, the nonlinearity of the effective diffusivities as functions of the input parameters, and the large number of parameters made a conventional uncertainty analysis infeasible. To incorporate the uncertainties in the input parameters into the calculations and obtain estimates of the uncertainties in the final results, we performed Monte Carlo calculations to determine the distribution in the final results based on the uncertainties in the input. The results of these calculations are given in Tables 3.1 and 3.2. The uncertainties in Table 3.1 mean that the average value of the diffusivity can be either multiplied or divided by the number in parentheses to get the range of values for the diffusivity. Further details of the Monte Carlo calculations, including typical histograms of the probability distributions of effective diffusivities and generation rates, are given in Appendix D.

With the exception of Tank A-101, the generation rates listed in Table 3.2 range from 3 to 100 g/day. The liquid layer in Tank A-101, however, is generating about 350 g/day, comparable to Tank SY-101, which has been estimated to generate ammonia at 600 g/day (Palmer et al. 1996). The effective diffusivities for ammonia in the nonconvective layers are reported in Table 3.1. The diffusivity of water is used as a scaling measure to provide an indication of how the calculated diffusivities compare with the diffusivity of ammonia in pure water. The results suggest that the diffusion of ammonia in the settled solids is almost identical to that of ammonia in pure water. However, if ammonia in a salt solution behaves according to the Stokes-Einstein relation (Hecht 1990), the diffusivity should scale according to the inverse of the viscosity. According to Reid et al. (1977), the molecular diffusivity of a solute in a nonelectrolytic solution is inversely proportional to the viscosity of the solvent. Recent nuclear magnetic resonance (NMR) experiments to determine the diffusion coefficient of ammonia in concentrated salt solutions indicate that the Stokes-Einstein relation also holds when the viscosity of the solution is increased by adding electrolyte (Bobroff et al. 1997). Because the viscosity of the supernatant liquid in the DSTs is approximately 20 cP (Stewart et al. 1996), one would expect a diffusivity of ammonia in the liquid portion of the waste that is 20 times less than that of water, provided the Stokes-Einstein relation holds. The effective diffusivities for the tanks would then all need to be multiplied by an additional factor of 20, indicating that the transport of ammonia is substantially higher than that expected from simple molecular diffusion in the liquid fraction of the waste.

The ammonia concentration distribution in A-101, S-106, and U-103 can be fit using the models described in Section 2. The effective diffusivity in the nonconvective layer of A-101 is higher than in any of the other tanks, suggesting that another mechanism, different from pure molecular diffusion in the liquid, is contributing to the transport of ammonia through the floating solids layer. The effective diffusivity of ammonia in the nonconvective layer in U-103 is comparable to the values seen in the DSTs. The effective diffusivity in the nonconvective layer in S-106 is

Table 3.1. Average Diffusivity Ratios

(D/D_{H2O})	AW-101	AN-103	AN-104	AN-105	A-101	S-106	U-103
Floating Solids	$17.1(2.5)^{\pm1}$	$13.0(3.5)^{\pm1}$	$5.7(3.4)^{\pm1}$	$21.3(2.6)^{\pm1}$	$73.8(1.5)^{\pm1}$	-	-
Settled Solids/Slurry	$2.1(2.5)^{\pm1}$	$1.8(3.4)^{\pm1}$	$2.5(3.2)^{\pm1}$	$16.2(2.5)^{\pm1}$	-	$0.5(2.0)^{\pm1}$	$4.9(1.5)^{\pm1}$

* The average value of the diffusivity can be either multiplied or divided by the number in parentheses to get the range of values for the diffusivity.

Table 3.2. Average Ammonia Generation Rates

Generation Rate (g/day)	AW-101	AN-103	AN-104	AN-105	A-101	S-106	U-103
Floating Solids	2.5±0.9	2.8±1.0	1.1±0.5	2.3±0.9	17.4±10	-	-
Liquid	22.5±8.2	12.0±4.1	13.6±6.3	41.2±16	353±260	0.9±0.3	-
Settled Solids/Slurry	9.4±3.5	9.8±3.3	9.9±4.6	30.3±12	-	2.7±0.8	98.1±36

considerably smaller than the values seen in either the DSTs or SSTs and is close to the expected value for the ammonia diffusivity in a concentrated electrolyte solution with a viscosity of 20 cP.

The following sections contain a more detailed discussion of the calculations for the DSTs and SSTs. The mean values reported in Tables 3.1 and 3.2 were obtained from Monte Carlo simulations by allowing all parameters to vary in the calculation. As discussed in Appendix D, the distributions for the effective diffusivities are lognormal. To get a better idea of how the effective diffusivities depend on the individual parameters, single point calculations were performed with all inputs set at their mean values. The values of the effective diffusivities calculated in this way are reported in Table 3.3 for a value of 1.0 for the concentration scale factor, f. Additional calculations were performed to examine the behavior of the diffusivities as functions of selected variables. These are also described in the following sections.

Table 3.3. Calculated Diffusivity Ratios for f = 1

(D/D_{H2O})	AW-101	AN-103	AN-104	AN-105	A-101	S-106	U-103
Floating Solids	33.2	26.5	12.6	75.2	606	-	-
Settled Solids/Slurry	4.5	4.7	6.9	44.6	-	0.5	4.9

3.1 Double-Shell Tanks

In this section, the calculated ammonia concentration distributions for Tanks AW-101, AN-103, AN-104, and AN-105 are presented. In addition, the behavior of the diffusivities in the nonconvective layers with respect to the scale factor f and the mass transfer coefficients are analyzed. The modeling results for Tank AW-101 are discussed in detail. For the remaining tanks, results are similar to those in Tank AW-101 and thus are summarized briefly. Figure 3.1 compares the calculated ammonia concentration distribution for two different values of the concentration correction factor f and the corresponding RGS values for Tank AW-101. It is important to note that the concentrations in the settled and floating solids layers are normalized by the liquid volume fraction; i.e., the units of concentration are μmole/L of liquid (μM) and not μmole/L of waste. Wilkins et al. (1997) reported an average dome space concentration of 7 ppm ammonia. Normalizing the effective diffusivities with that of water (2×10^{-9} m^2/s), when f = 1, the diffusivity ratios for the floating solids and nonconvective solids layers are 33 and 5, respectively. If f is increased to 3, the effective diffusivity ratios for the floating solids and settled solids layers drop to 10 and 2. The effective diffusivities appear to scale approximately as the inverse of the scale factor, f.

For the present model, sensitivity studies indicate that if the concentrations in the waste increase, the diffusivities must decrease to maintain the same ammonia concentration at the dome space. The diffusivities in the nonconvective layers are monotonically decreasing functions of the concentration correction factor, as illustrated in Figure 3.2 for Tank AW-101. Similar results were obtained for the other DSTs, with the exception of Tank AN-105, which behaves slightly differently. The diffusivities shown in Figure 3.2 assume that the generation rates for each of the layers remain fixed.

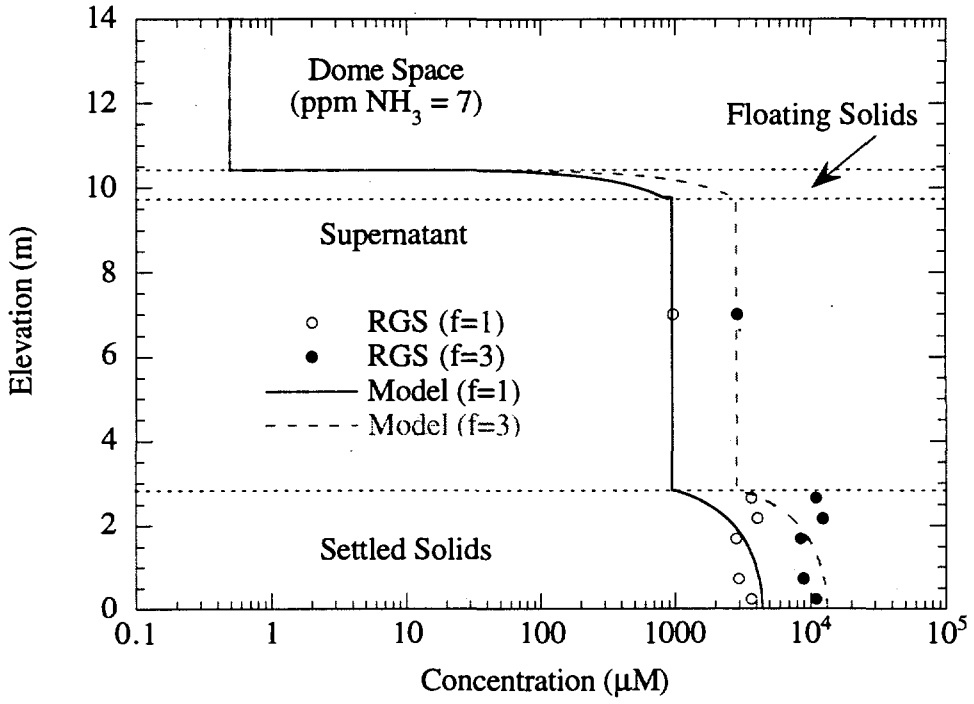

Figure 3.1. Ammonia Concentration Distribution in Tank AW-101 (model Eq. 2.1–2.8)

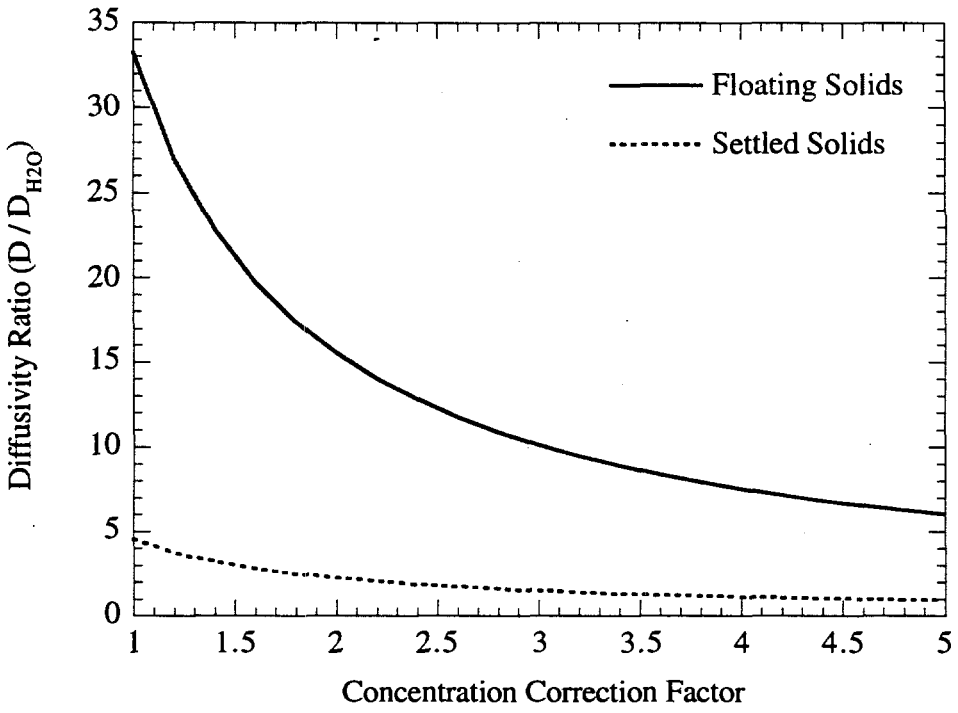

Figure 3.2. Diffusivity Ratios for Nonconvective Layers as a Function of the Concentration Correction Factor in Tank AW-101

Figure 3.3 shows how the diffusivities vary as a function of the mass transfer coefficients, h_{sl} and h_{lc}, over two decades. The figure shows that the diffusivities are relatively insensitive to increases in the mass transfer coefficient. The effective diffusivity in the floating solids layer, however, appears to be sensitive to decreases in the mass transfer coefficient and significant changes in the effective diffusivities may result if the mass transfer coefficients have been overestimated. The insensitivity to increases in the mass transfer coefficient follows from the fact that rapid transport of ammonia from the top of the settled solids layer to the bottom of the floating solids layer effectively enforces a continuity condition on the ammonia concentration in these two layers that are independent of further increases in the mass transfer rate.

A comparison between the RGS data for Tank AN-103 and the model results calculated using f = 1 are shown in Figure 3.4. RGS ammonia data for Tank AN-103 were scarce, and no specific average value is known for the dome space concentration. Wilkins et al. (1997) provided an upper bound of 10 ppm for ammonia in the dome space. For these calculations, an average value of 5 ppm was assumed. The model does a good job of matching the measured concentrations in the supernatant and settled solids layer but appears to significantly underestimate the ammonia concentration in the floating solids layer. The diffusivities calculated for AN-103 have the same qualitative dependence on the scale factor f seen in Tank AW-101.

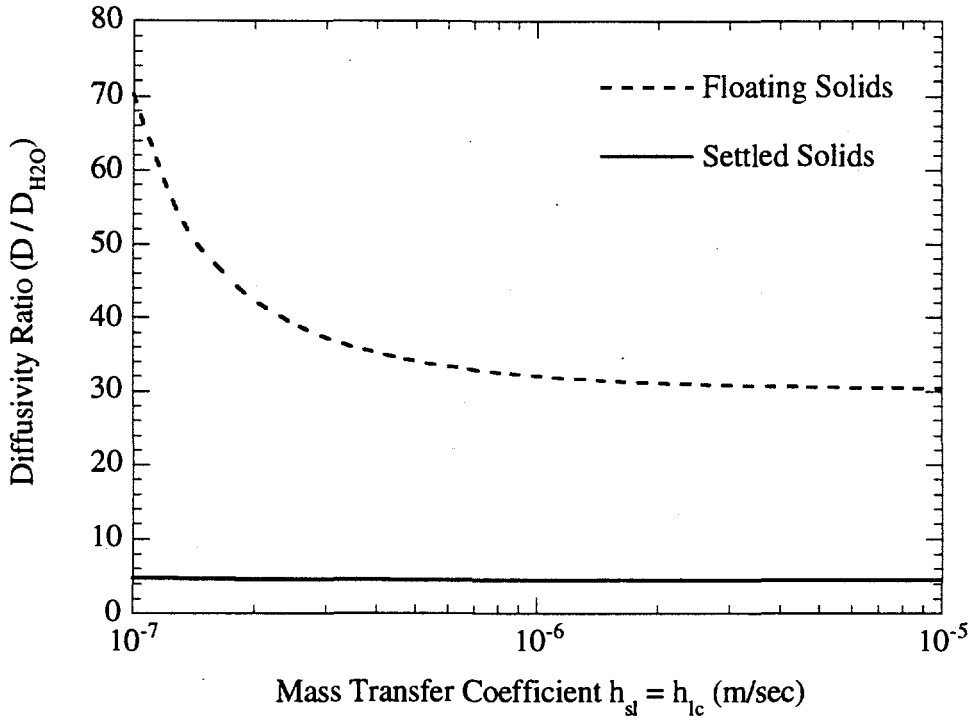

Figure 3.3. Diffusivity Ratios for Nonconvective Layers as a Function of the Mass Transfer Coefficient in Tank AW-101

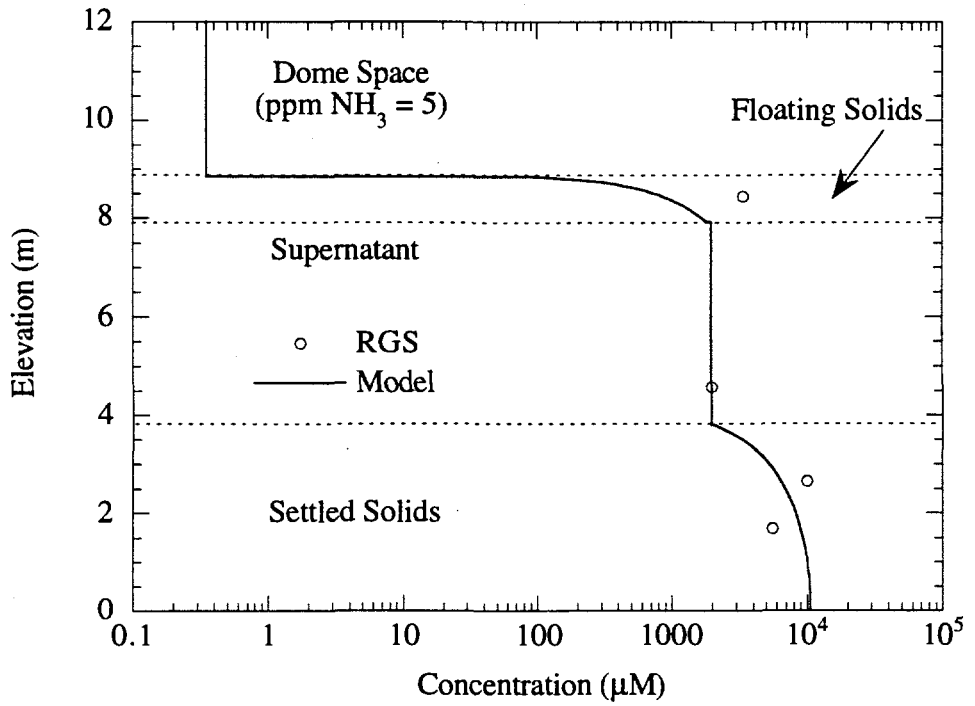

Figure 3.4. Ammonia Concentration Distribution in Tank AN-103 (model Eq. 2.1–2.8)

The RGS ammonia data for Tank AN-104 are plotted in Figure 3.5 along with the results of fitting the model for f = 1. As with AN-103, only an upper bound of 10 ppm is reported for the ammonia dome space concentration in Tank AN-104 (Wilkins et al. 1997). For the calculations, a value of 5 ppm was assumed. The behavior of the diffusivities with respect to the scale factor is very similar to that seen in Tanks AW-101 and AN-103.

Tank AN-105 appears more anomalous in its behavior than the other DSTs. The RGS ammonia data for Tank AN-105 are plotted in Figure 3.6 along with the model fit for f = 1. The average ammonia dome space concentration in Tank AN-105 is 15 ppm (Wilkins et al. 1997). Unlike the previous tanks, there is a noticeable discontinuity in the concentration at the supernatant-floating solids and settled solids-supernatant interfaces. This suggests that the diffusivities for Tank AN-105 will be much more sensitive to the values of the mass transfer coefficients. Figure 3.7 shows how the diffusivity ratio of the floating solids layer decreases rapidly (from 350 to 50) over an order of magnitude change in the mass transfer coefficients ($h_{sl} = h_{lc}$), and finally a plateau (at 40) is reached for larger values of the transfer coefficients. For a two order-of-magnitude change in the transfer coefficients, the settled solids layer diffusivity ratio merely decreases by 10%. Figure 3.8 shows the variation of the diffusivity ratios for the floating and settled solids layers as a function of the correction factor f. Notice that the diffusivity of the floating solids layer decays rapidly for f larger than unity (at f = 1, ratios for floating and settled solids layers are 75 and 45, respectively). For f = 3, the diffusivity ratios in both the floating and settled solids layers drop to 13 and 14, respectively. In addition, for values of f greater than 2.5 the settled solids layer diffusivity ratio (16) is slightly higher than that of the floating solids layer (15). If the values for the ammonia concentration are accurate, the transport of ammonia in this tank appears to be very fast. However, if the RGS values underestimate the values of the ammonia concentration, the transport of ammonia in this tank compares with that in the other DSTs.

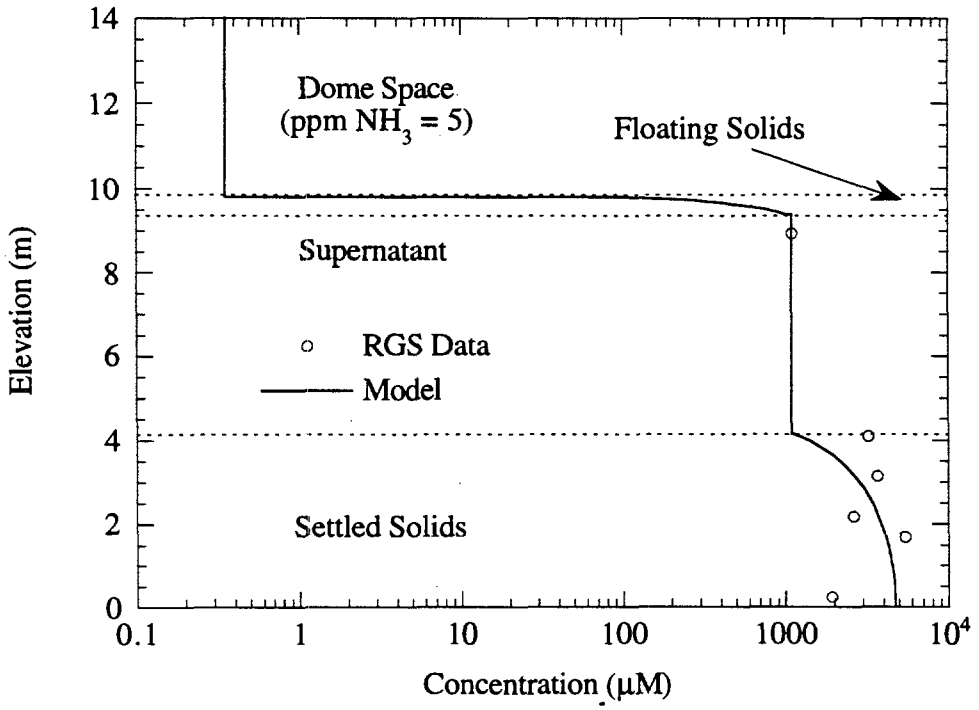

Figure 3.5. Ammonia Concentration Distribution in Tank AN-104 (model Eq. 2.1–2.8)

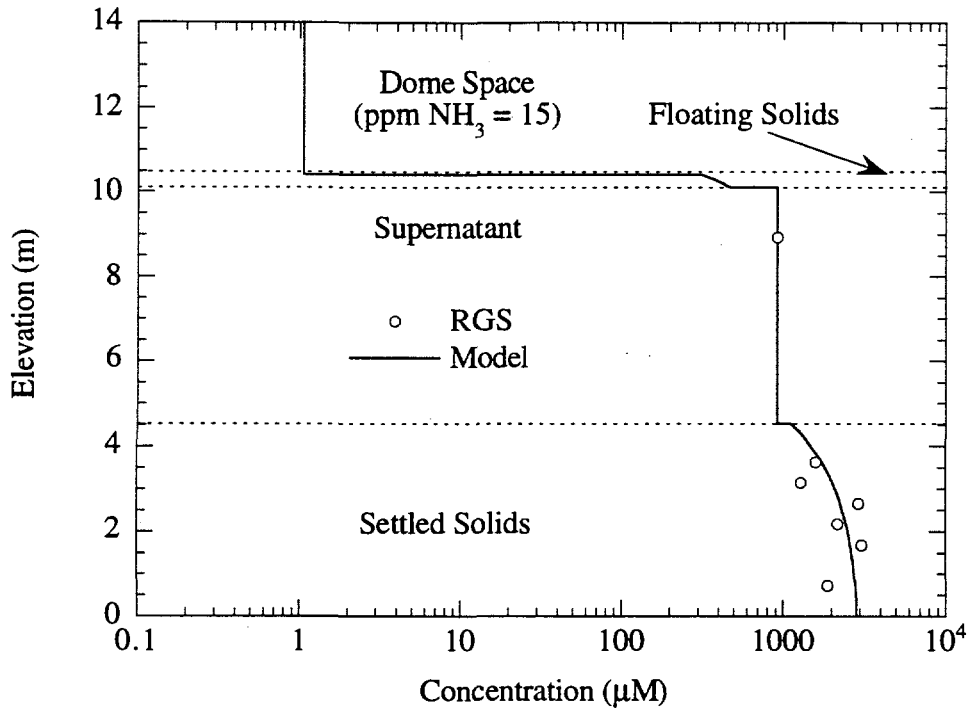

Figure 3.6. Ammonia Concentration Distribution in Tank AN-105 (model Eq. 2.1–2.8)

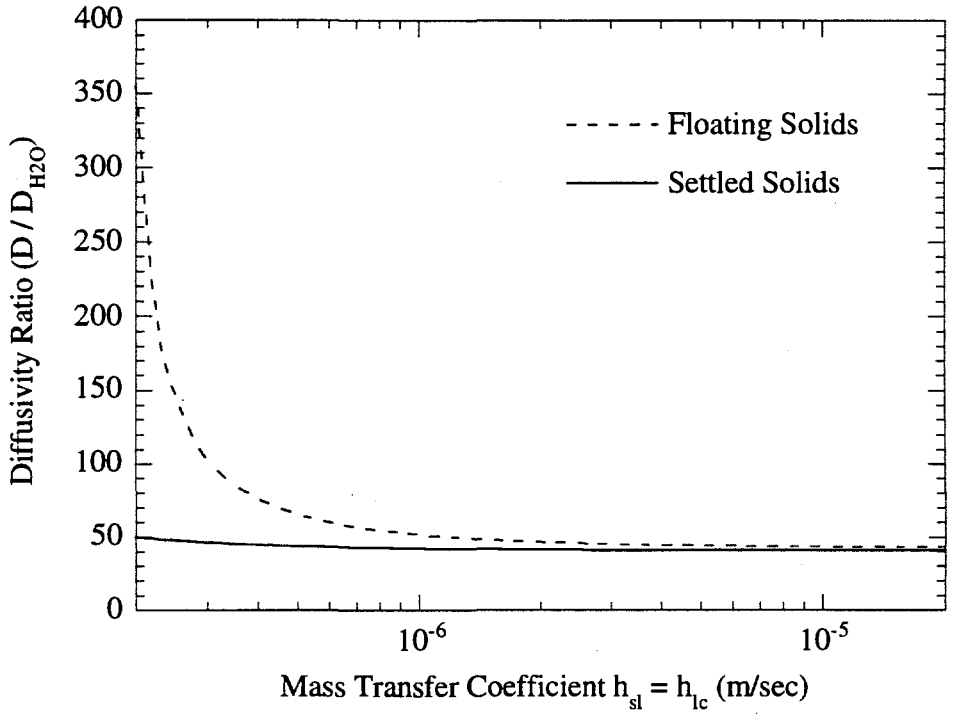

Figure 3.7. Diffusivity Ratios for Nonconvective Layers as a Function of the Mass Transfer Coefficient in Tank AN-105

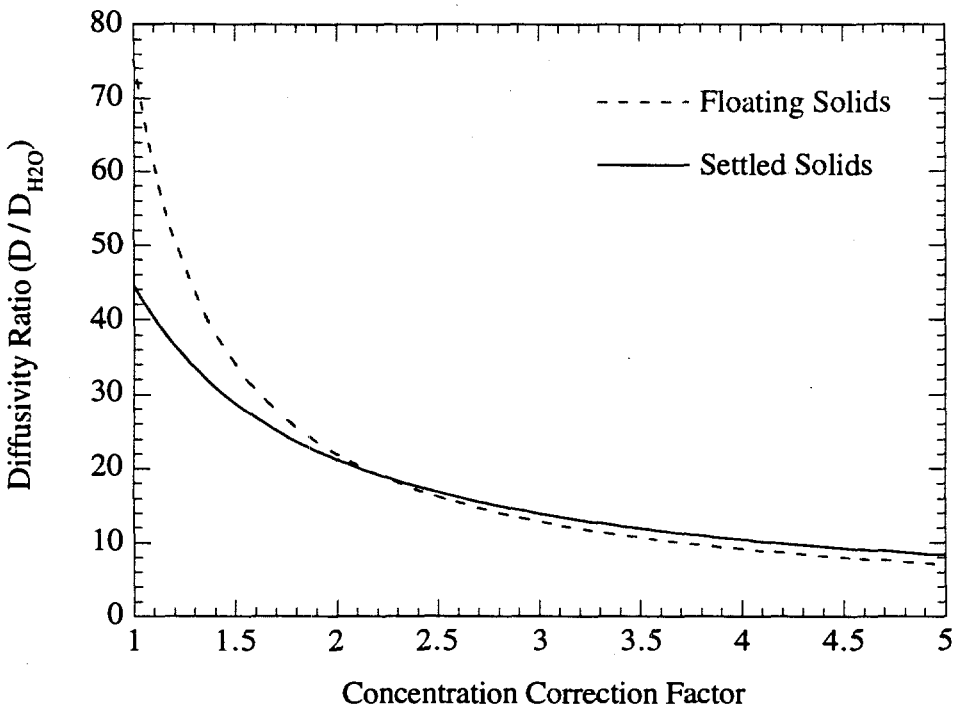

Figure 3.8. Diffusivity Ratios for Nonconvective Layers as a Function of the Concentration Correction Factor in Tank AN-105

3.2 Single-Shell Tanks

In this section, results on the modeled ammonia concentration distribution for SSTs A-101, S-106, and U-103 are presented. For Tank A-101, the average dome space concentration is 750 ppm. Figure 3.9 shows that the calculated and measured distributions of ammonia are in good agreement. The calculated distribution reproduces the average concentrations in each layer, which is not surprising since these concentrations were used as inputs to the fit, but it also approximately reproduces the slope of the concentration gradient in the floating nonconvective layer.

Figure 3.10 shows the behavior of the effective diffusivity as a function of the concentration correction factor. The effective diffusivity for this tank is an extremely sensitive function of the scale factor f for this tank and appears to scale more rapidly than the inverse of f. A factor of two increase in the concentrations would result in approximately a seven-fold decrease in the effective diffusivity.

For Tank S-106, the average ammonia dome space concentration is 36.5 ppm. Figure 3.11 compares the reported RGS data and the model results (Eq. 2.14–2.18) of the ammonia concentration distribution. Notwithstanding the simplifying assumptions used in the governing equations (i.e., the waste stratification can be modeled with two layers; the presence of a partial floating solids layer and the three-dimensional character of the stratification can be neglected) and the limited number of data points, the results show that the simple model approximately accounts for the concentration distribution.

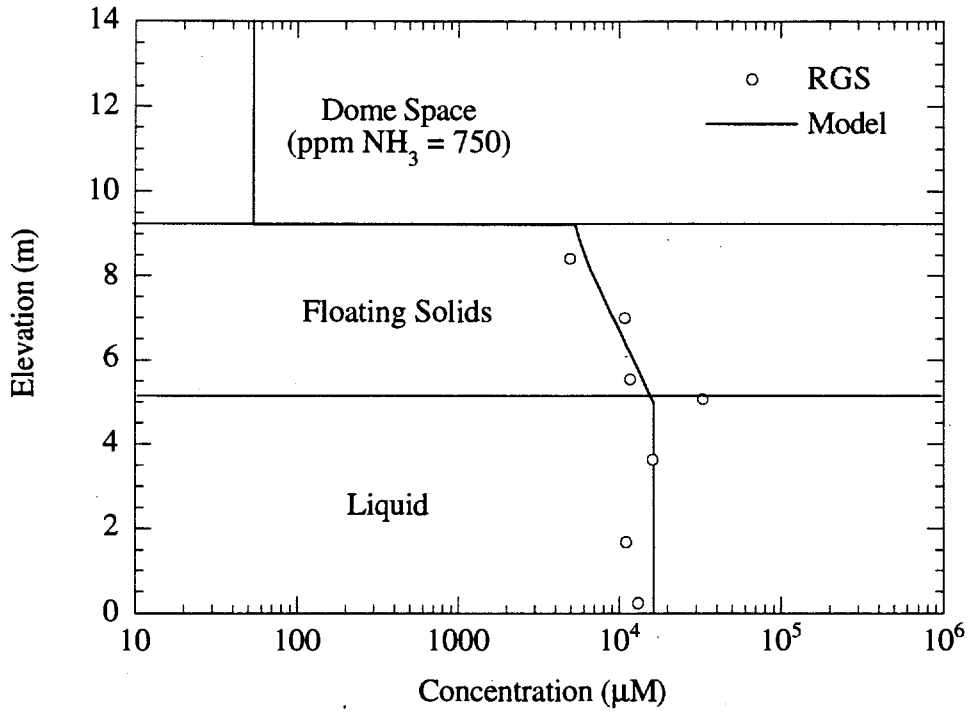

Figure 3.9. Ammonia Concentration Distribution in Tank A-101 (model Eq. 2.9–2.13)

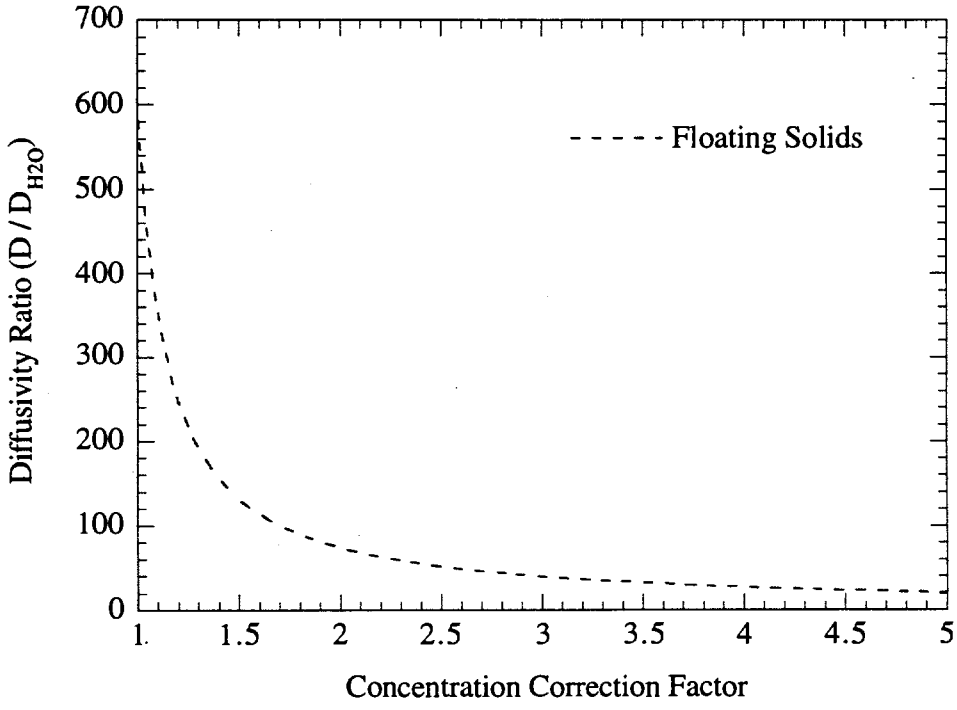

Figure 3.10. Diffusivity Ratio for the Floating Solids Layer as a Function of the Concentration Correction Factor in Tank A-101

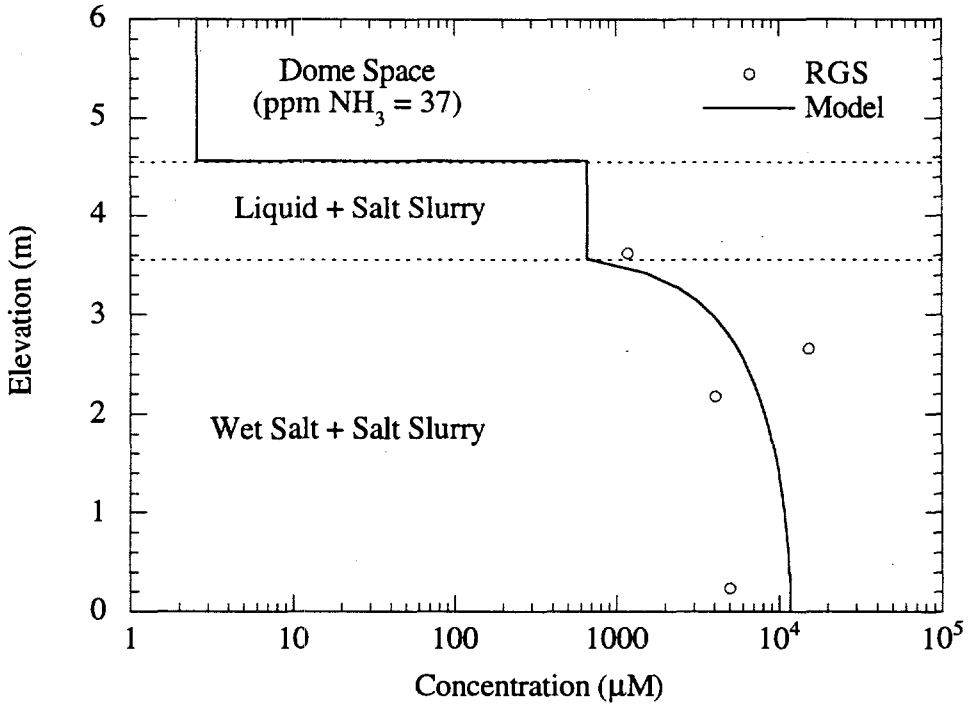

Figure 3.11. Ammonia Concentration Distribution in Tank S-106 (model Eq. 2.14–2.18)

In Tank U-103, the average ammonia dome space concentration is 736 ppm. Figure 3.12 compares the reported RGS data and the model results for the ammonia concentration distribution. The agreement between the model and the measured distribution is reasonable, although the model appears to severely overestimate the concentration of ammonia near the top of the tank.

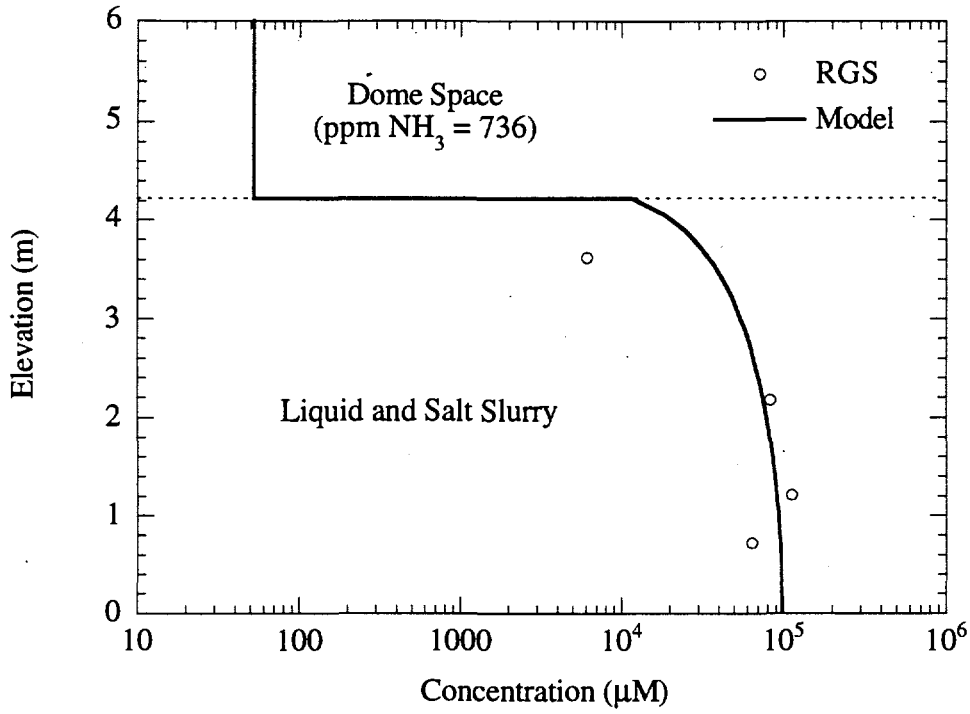

Figure 3.12. Ammonia Concentration Distribution in Tank U-103 (model Eq. 2.19–2.22)

4.0 Conclusions

The fits of the DSTs ammonia profiles to a simple one-dimensional model of ammonia transport via convection and diffusion indicate that the ammonia profiles in most cases are consistent with current ideas about ammonia generation and transport within the waste tanks. The difference between the ammonia concentration measured in the waste and that which would be predicted based on measurements in the dome space of the DSTs can be completely explained by the finite ventilation rate of the dome space and the transport barrier to ammonia release represented by the floating solids layer. The fits also suggest that transport of ammonia in the DST settled solids and floating solids layers is faster than expected for pure diffusion, especially if the molecular diffusivity in the liquid portion of the waste is scaling as the inverse of the viscosity. These enhanced diffusivities may point to the presence of additional transport mechanisms such as bubble-assisted transport or slow motion of the interstitial liquid induced by thermal gradients in the nonconvective layers.

Although the DST model contains many parameters, most of them can be fixed using information about the tank geometry and waste configuration. The remaining parameters can be estimated using known values from previous waste samples. For these calculations only the diffusion coefficients of ammonia in the nonconvective layers were treated as adjustable parameters. This suggests a possible path for estimating ammonia concentrations for tanks in which the waste configuration is known but only dome space measurements of the ammonia concentration are available. If the diffusion coefficients for ammonia in the nonconvective waste layers and the Henry's Law constants can be estimated for these tanks, then the ammonia profile can be calculated from the dome space ammonia concentration. The results for the DSTs suggest that a generic value for the diffusivity ratio in the floating solids layer is about 6–20, and a generic value for the settled solids layer is about 2. These values could be used as the basis for an estimate of the ammonia inventory in the entire tank, provided a headspace ammonia measurement is available and the configuration of waste in the tank is known. Information on in-waste ammonia concentrations could be obtained for additional tanks for which headspace measurements are available.

Modeling the SSTs gave more variable results than modeling the DSTs, partly because of the differences in the waste configurations of the SSTs. Unlike the DSTs, which can all be described by a single model, the SSTs required three separate models for the three tanks examined in this study. The most atypical of the SSTs was Tank A-101 which has a floating nonconvective layer on top of a convective liquid layer. Modeling of this tank suggests that the transport of ammonia through the nonconvective layer is very fast and that mechanisms other than molecular diffusion are playing a significant role. The effective diffusivity for this layer is about a factor of 5 larger than the effective diffusivities seen in any of the settled solids layers for the DSTs. Results for Tank S-106 indicate that transport through the nonconvective layer settled solids layer of this tank could be characterized almost completely by molecular diffusion, while results for Tank U-103 give an effective diffusivity in the nonconvective layer that is comparable to the effective diffusivity in the settled solids layers of the DSTs. Because results are available for only a few SSTs, it is not possible to say whether estimates of in-waste ammonia concentrations based on head space ammonia measurements would be feasible.

5.0 References

Bobroff S, RJ Phillips, and A Shekarriz. 1997. *Nuclear Magnetic Resonance Measurement of Ammonia Diffusion in Dense Solid-Liquid Slurries.* PNNL-11678, Pacific Northwest Northwest Laboratory, Richland, Washington.

Brevick CH, LA Gaddis, and W Pickett. 1994. *Historical Tank Content Estimate for the South West Quadrant of the Hanford 200 West Area.* WHC-SD-WM-ER-352, Westinghouse Hanford Company, Richland, Washington.

Bryan SA, CM King, LR Pederson, SV Forbes, and RL Sell. 1996. *Gas Generation from Tank 241-SY-103 Waste.* PNL-10978, Pacific Northwest Laboratory, Richland, Washington.

Bryan SA and LR Pederson. 1996. *Thermal and Combined Thermal and Radiolytic Reactions Involving Nitrous Oxide, Hydrogen, Nitrogen, and Ammonia in Contact with Tank 241-SY-101 Simulated Waste.* PNL-10748, Pacific Northwest Laboratory, Richland, Washington.

Cussler EL. 1984 *Diffusion Mass Transfer in Fluid Systems.* Cambridge University Press, London.

Field JG, DE Place, and RD Cromar. 1997. *Tank Characterization Report for Single-Shell Tank 241-A-101.* HNF-SD-WM-ER-673 Rev. 0, Lockheed Martin Hanford Corp., Richland, Washington.

Hecht CE. 1990. *Statistical Thermodynamics and Kinetic Theory.* WH Freeman and Co., New York.

Hodgson KM, RP Anantamula, SA Barker, KD Fowler, JD Hopkins, JA Lechelt, and DA Reynolds. 1996. *Evaluation of Hanford Tanks for Trapped Gas.* WHC-SD-WM-ER-526 Rev. 1, Westinghouse Hanford Company, Richland, Washington.

Huckaby JL, KB Olsen, DS Sklarew, JC Evans, and KM Redmund. 1997. *Measurements of Waste Tank Passive Ventilation Rates Using Tracer Gases.* PNNL-11683, Pacific Northwest National Laboratory, Richland, Washington.

Lilga MA, RT Hallen, EV Anderson, MO Hogan, TL Hubler, GL Jones, DJ Kowalski, MR Lumetta, WF Riemath, RA Romine, GF Schiefelbein, and MR Telander. 1996. *Ferrocyanide Aging Studies.* PNNL-11211, Pacific Northwest National Laboratory, Richland, Washington.

Meyer PA, ME Brewster, SA Bryan, G Chen, LR Pederson, CW Stewart, and G Terrones. 1997. *Gas Retention and Release Behavior in Hanford Double-Shell Waste Tanks.* PNNL-11536 Rev. 1, Pacific Northwest National Laboratory, Richland, Washington.

Palmer BJ, CM Anderson, G Chen, JM Cuta, TA Ferryman, and G Terrones. 1996. *Evaluation of the Potential for Significant Ammonia Releases from Hanford Waste Tanks*. PNNL-11237, Pacific Northwest National Laboratory, Richland, Washington.

Reid RC, JM Prausnitz, and TK Sherwood. 1977. *The Properties of Liquids and Gases, 3rd ed.* McGraw-Hill, New York.

Shekarriz A, DR Rector, LA Mahoney, MA Chieda, JM Bates, RE Bauer, NS Cannon, BE Hey, CG Linschooten, FJ Reitz, ER Siciliano. 1997. *Composition and Quantities of Retained Gas Measured in Hanford Waste Tanks 241-AW-101, A-101, AN-105, AN-104, and AN-103*. PNNL-11450 Rev. 1, Pacific Northwest National Laboratory, Richland, Washington.

Stewart CW, JM Alzheimer, ME Brewster, G Chen, RE Mendoza, HC Reid, CL Shepard, and G Terrones. 1996. *In Situ Rheology and Gas Volume in Hanford Double Shell Waste Tanks*. PNNL-11296, Pacific Northwest National Laboratory, Richland, Washington.

Wilkins NE, RE Bauer, and DM Ogden. 1997. *Results of Vapor Space Monitoring of Flammable Gas Watch List*. HNF-SD-WM-TI-797 Rev. 1, Lockheed Martin Hanford Corporation, Richland, Washington.

Appendix A

Estimate of Mass Transfer Coefficients

Appendix A

Estimate of Mass Transfer Coefficients

To estimate the overall mass transfer coefficients it is necessary to normalize the effective Henry's Law constants in terms of the water content for each layer of waste. These values were obtained by converting the Henry's Law constants from units of moles/kg-waste-atm to moles/kg-H_2O-atm using the values of the densities for the settled solids layer, the supernatant, and the floating solids layer (when available) as well as the appropriate water fractions, and then taking the average. The Henry's Law constants for the DSTs (as reported by Shekarriz et al. [1997]) are highly uncertain and could vary by a factor of up to nine, whereas for the SSTs they could vary by a factor of two.

The average Ostwald solubility coefficient λ (Glasstone 1954) is calculated from the normalized effective Henry's constant K_H (in moles/kg-H_2O-atm) from

$$\lambda = \frac{R\rho_l\omega_l}{H}\int_0^H T(z)K_H(z)dz$$

where

R = universal gas constant
H = height of the waste (in m)
T = absolute temperature (in K)
ρ_l = density of the liquid (in kg/m^3)
ω_l = mass fraction of water in the liquid.

For the settled solids layers in DSTs, the liquid volume fractions υ_x (x = settled solids (s) or floating solids (c)) are given by

$$\upsilon_x = (1-\gamma_x)(1-\sigma_x')$$

where

γ_x = gas volume fraction at the x layer
σ_x' = solids volume fraction on a gasless basis at the x layer (as reported by Shekarriz et al. 1997).

Assuming that the ratio between the solids volume fraction and the liquid volume fraction β (σ_s/υ_s) in the settled solids layer is the same as that in the floating solids in DSTs, the liquid volume fractions, υ_c, are approximated by

$$\upsilon_c = \frac{1-\gamma_c}{1+\beta}$$

The mass fractions of water in the liquid ω_l were obtained from measurements reported in the Tank Characterization Reports (TCR) (Field 1997; Jo 1997; Baldwin 1995) and RGS estimates (Shekarriz et al. 1997). The mass fractions of water in the settled solids (x = s) and floating solids (x = c) are

$$\omega_x = \frac{\rho_l}{\rho_x}\omega_l \upsilon_x$$

Following the procedure outlined by Palmer et al. (1996), the overall mass transfer coefficient at the fluid-saturated, floating solids-gas interface, h_{ca}, can be derived by assuming that the concentration of ammonia flowing out of the tank headspace due to ventilation is equal to the flux of ammonia to the surface of the waste:

$$QC_a = -A\frac{D_c}{\upsilon_c}\frac{dC_c}{dz}\bigg|_{z=L} \tag{A.1}$$

and that the concentration of ammonia at the upper surface of the floating solids is in equilibrium with the concentration of ammonia in the headspace

$$\lambda C_a = \frac{C_c(L)}{\upsilon_c} \tag{A.2}$$

Here L is taken to refer to the top of the waste. These conditions can be recast as mass transfer relations having the form

$$A h_{ca}\left[\frac{C_c(L)}{\upsilon_c} - C_a\right] = QC_a \tag{A.3}$$

$$h_{ca}\left[\frac{C_a(L)}{\upsilon_c} - C_a\right] = -\frac{D_c}{\upsilon_c}\frac{dC_c}{dz}\bigg|_{z=L} \tag{A.4}$$

Equation (A.1) can be recovered from (A.3) and (A.4) by dividing (A.4) by A and eliminating the bracketed term from the two equations. An analytic expression for the mass transfer coefficient h_{ca} can be obtained by solving Equation (A.3) for $C_c(L)/\upsilon_c$ and setting the result equal to λC_a using Equation (A.2). The resulting expression can then be solved for h_{ca} to get

$$h_{ca} = \left[\frac{Q}{A(\lambda - 1)}\right]$$

The calculation of the gas-liquid mass transfer coefficient h_{la} is accomplished by assuming that convection overwhelms diffusion except on a timescale shorter than τ_c, the timescale for convection in the liquid. The concentration in the liquid layer decays from the average value in the liquid C_l to λC_a over a distance $\sqrt{D\tau_c}$. Over the short distance and times involved, the

concentration in the thin layer at the surface of the liquid can be considered to be diffusing at steady state, implying that the concentration profile in the boundary is linear. The linear profile can be combined with the boundary conditions at both ends of the diffusion layer to relate C_a and C_l. Following a procedure similar to the calculation of h_{ca}, and estimating τ_c by L_l/U, where L_l is the thickness of the convective layer and U is the mean fluid velocity in the convective layer, the overall mass transfer coefficient, h_{la}, at the gas-liquid interface is

$$h_{la} = \left[\frac{A(\lambda - 1)}{Q} + \sqrt{\frac{L_l}{UD_l}} \right]^{-1}$$

To obtain the mass transfer coefficients for the fluxes between the liquid layers and the floating and settled solids layers, the analogy between heat and mass transfer is exploited. A one-to-one correspondence between a convective heat transfer and a convective mass transfer problem can be established when the flow pattern is the same and the dimensionless equations and boundary conditions are mathematically equivalent (White 1988). Therefore, an estimate of the overall mass transfer coefficients at the settled solids-liquid interface, h_{sl}, and at the liquid-floating solids interface h_{lc}, can be obtained by applying the mass transfer analogy to an experimental correlation for the analogous heat transfer problem. Furthermore, assuming that the structures of the floating solids and settled solids layers are similar, h_{sl} and h_{lc} can be expected to have the same order of magnitude. In the present calculations, it is assumed that both transfer coefficients have the same numerical value for the DSTs.

It is assumed that the transport of ammonia takes place along a flat interface in which the characteristic velocity is imposed by buoyancy-driven convection due to a thermal gradient. Because the settled solids layer generates ammonia, there is a constant mass flux at the interface. Turbulent convective motion in the supernatant transports ammonia throughout this layer. The process by which ammonia is transferred through the settled solids-supernatant or supernatant-floating solids interfaces can be approximated by a turbulent convective mass transfer process over a flat plate with a constant mass flux. Applying the heat and mass transfer analogy to the turbulent boundary layer flow with constant heat flux (White 1988) yields the nondimensional relationship,

$$Sh_L = 0.0385 Re_L^{4/5} Sc$$

where

Sh_L = Sherwood number (hL/D_l)

Re_L = Reynolds number (UL/ν_l)

Sc = Schmidt number (ν_l/D_l).

The diffusivity of small molecules in aqueous solution ranges from approximately 1 to 2 x 10^{-9} m^2/s for almost all small solutes (Cussler 1984). There is experimental evidence that for nonelectrolytic solutions the diffusion coefficient is inversely proportional to the viscosity of the solvent, and that for electrolytic solutions the diffusivity decreases with increasing salt concentration (Reid et al. 1977; Bobroff et al. 1997). Therefore, the expected value of molecular diffusivity for ammonia in the liquid waste will be smaller than in water. To estimate the diffusivity of ammonia D_l in a liquid waste, the following expression is used:

$$D_l = \frac{\mu_{H_2O}}{\mu_l} D_{H_2O}$$

where μ_{H_2O} is 1 cP and D_{H_2O} is 2 x 10^{-9} m^2/s.

A characteristic convective velocity U can be obtained by equating the kinetic energy per unit volume to the work per unit volume caused by buoyancy (Gebhart et al. 1988):

$$U = \sqrt{\frac{2gL_l(\rho_{top} - \rho_{bottom})}{\rho_{bottom}}}$$

where

ρ_{top} = density at the top of the supernatant layer,

ρ_{bottom} = density at the bottom of the supernatant layer

Assuming that the thermal expansion coefficient of liquid waste behaves the same as that for water, the density variation (in kg/m^3) as a function of temperature (in °C) is

$$\rho_l(T) = SG_l\left(1000 + 2.846x10^{-2}\,T - 6.33x10^{-3}\,T^2 - 1.982x10^{-5}\,T^3\right)$$

where SG_l is the specific gravity of the liquid waste, and 5°C <T <70°C. The above correlation was obtained by applying a least squares fit to data provided by Batchelor (1967).

The parameter ν_l (used in the Reynolds number and the Schmidt number) is the kinematic viscosity of the liquid (in m^2/s). The length of a convection cell (1.17 L_l; see Chandrasekhar 1981) is used as the length scale L along the horizontal direction for both the Sherwood number and the Reynolds number. Therefore, the mass transfer coefficients h_{sl} and h_{lc} are

$$h_{sl} = h_{lc} = 0.0373\left(\frac{D_l}{L_l}\right)\left(\frac{\nu_l}{D_l}\right)^{1/3}\left(\frac{UL_l}{\nu_l}\right)^{4/5}$$

References

Baldwin JH. 1995. *Tank Characterization Report for Double-Shell Tank 241-AW-101.* HNF-SD-WM-ER-470, Westinghouse Hanford Company, Richland, Washington.

Batchelor GK. 1967. *An Introduction to Fluid Dynamics.* Cambridge University Press, London.

Bobroff S, KJ Phillips, and A Shekarriz. 1997. *Nuclear Magnetic Resonance Measurement of Ammonia. Diffusion in Dense Solid-Liquid Slurries.* PNNL-11678, Pacific Northwest National Laboratory, Richland, Washington.

Chandrasekhar S. 1981. *Hydrodynamic and Hydromagnetic Stability*. Dover Publications Inc., New York.

Cussler EL. 1984. *Diffusion Mass Transfer in Fluid Systems*. Cambridge University Press, Cambridge, UK.

Field JG. 1997. *Tank Characterization Report for Single-Shell Tank 241-A-101*. HNF-SD-WM-ER-673, Lockheed Martin Hanford Corporation, Richland, Washington.

Gebhart B, Y Jaluria, RL Mahajan, and B Sammankia. 1988. *Buoyancy-Induced Flows and Transport*. Hemisphere Publishing Corporation, New York.

Glasstone S. 1954. *Textbook of Physical Chemistry*. D. Van Nostran Company Inc., New York.

Jo J. 1997. *Tank Characterization Report for Double-Shell Tank 241-AN-105*. HNF-SD-WM-ER-678, Lockheed Martin Hanford Corporation, Richland, Washington.

Palmer BJ, CM Anderson, G Chen, JM Cuta, TA Ferryman, and G Terrones. 1996. *Evaluation of the Potential for Significant Ammonia Releases from Hanford Waste Tanks*. PNNL-11237, Pacific Northwest National Laboratory, Richland, Washington.

Reid RC, JM Prausnitz, and TK Sherwood. 1977. *The Properties of Liquids and Gases, 3rd ed.* McGraw-Hill, New York.

Shekarriz A, DR Rector, LA Mahoney, MA Chieda, JM Bates, RE Bauer, NS Cannon, BE Hey, CG Linschooten, FJ Reitz, and ER Siciliano. 1997. *Composition and Quantities of Retained Gas Measured in Hanford Waste Tanks 241-AW-101, A-101, AN-105, AN-104, and AN-103*. PNNL-11450 Rev. 1, Pacific Northwest National Laboratory, Richland, Washington.

White FM. 1988. *Heat and Mass Transfer*. Addison-Wesley Publishing Co., New York.

Appendix B

Convection in the Liquid, Floating Solids, and Settled Solids Layers

Appendix B

Convection in the Liquid, Floating Solids, and Settled Solids Layers

Measurements in Tanks AW-101, AN-103, AN-104, and AN-105 indicate that there is no appreciable temperature difference between the settled solids-supernatant interface and the supernatant-floating solids interface (Meyer et al. 1997; Stewart et al. 1996). In Tank A-101 the temperature distribution in the liquid layer (from riser 10) appears to be convectively stable. Temperatures from the multi-instrument thermocouple trees (MITs) or old thermocouple trees are not sufficiently accurate (± 3 to 4°C). However, these liquid layers are convective because there are regions with convectively unstable temperature gradients. Therefore, we assign an equivalent unstable temperature difference of 1 to 5°C as the driving component of convection in these layers. When a fluid layer is heated from below, buoyancy-driven convection will occur if the Rayleigh number for the layer exceeds 1100 (Chandrasekhar 1981). The Rayleigh number Ra is defined as

$$Ra = \frac{\beta_l \, \Delta T \rho_l \, g \, L_l^3}{\kappa_l \, \mu_l} \qquad (B.1)$$

where

β_l = thermal expansion coefficient (in 1/°C)

ΔT = temperature difference between the bottom and the top of the fluid layer (in °C)

ρ_l = density (in kg/m^3)

κ_l = thermal diffusivity (in m^2/s)

μ_l = viscosity (in Pa-sec).

Using the respective densities, viscosities, and depths of the liquid layer for the tanks in question and the thermophysical properties of water for β_l and κ_l, the Rayleigh numbers are greater than 10^{12} for the assumed temperature differences range. This means that for these conditions, the buoyancy-driven flow in the liquid layers of each tank will be in the turbulent regime.

The floating solids layer consists of a combination of settled solids, supernatant fluid, and a sufficient amount of insoluble gas bubbles that make it buoyant. For the purpose of analysis, this layer is regarded as a supernatant-saturated porous medium (in reality the settled solids and floating solids layers are somewhat porous). A similar convective stability criterion exists in the case of a fluid-saturated porous layer heated from below (Katto and Masuoka 1967). A layer is unstable if the Rayleigh number, R_C, is greater than 39.5. R_C is defined as

$$R_C = \frac{P\beta_l \, \Delta T \rho_l^2 \, g \, c_{pl} \, L_l}{k_m \, \mu_l} \qquad (B.2)$$

where

P = permeability of the porous layer (in m^2)

c_{pl} = specific heat capacity of the liquid (in W/m^3)

k_m = combined thermal conductivity of the floating solids layer and liquid (in W/m-°C).

Using an upper bound on the temperature jump of 10°C across the floating solids layer, and assuming that the thermophysical properties for nonmetallic solids apply to the floating solids layer and that the permeability ranges from 10^{-10} to 10^{-12} m^2 (there are no experimental measurements of permeability for the tanks we studied; however, a typical value of permeability in ferrocyanide waste of 10^{-12} was reported by McGrail et al. 1993), the R_c values for the floating solids layers of the tanks under consideration are smaller than the critical value for convection. Therefore, bulk motion of liquid in the floating solids layers is not expected.

The settled solids layer at the bottom of the DSTs consists of a combination of sedimented material, supernatant fluid, and insoluble gas bubbles. For the purpose of analysis, this layer is regarded as a supernatant-saturated porous medium with internal heat generation. Temperature distributions in the settled solids layer of DSTs have been found to be approximately parabolic. Therefore, the rate $\dot{q}_s$, at which energy is generated per unit volume (in W/m^3), can be estimated from the energy equation applied to the settled solids layer as

$$\dot{q}_s = \frac{2\varphi_s}{L_{max}(L_s - L_{max})}\left[T_{max} - T_0 + \frac{L_{max}(T_0 - T_l)}{L_s}\right] \qquad (B.3)$$

where

φ_s = thermal conductivity of the settled solids layer (in W/m-°C)

L_{max} = elevation at which the maximum temperature occurs

T_0 = temperature at the bottom of the settled solids layer (in °C)

T_l = temperature at the top of the settled solids layer (in °C)

T_{max} = maximum temperature in the layer.

Convection of a fluid in a porous medium subjected to internal heat generation occurs whenever the modified Rayleigh number R_S exceeds the value of 31 (Tveitereid 1977). The modified Rayleigh number is given by the relation

$$R_S = \frac{P\beta_l g \dot{q}_s L_s^3}{2c_{pl}\kappa_s^2 \mu_l} \qquad (B.4)$$

where κ_S = thermal diffusivity of the porous layer (in m^2/s).

Using the measured temperature distributions in the settled solids layers of the four DSTs (Shekarriz et al. 1997), and assuming that thermophysical properties for nonmetallic solids apply to the settled solids and that the permeability is on the order of 10^{-12} m^2 (McGrail et al. 1993), the

modified Rayleigh numbers for the settled solids layers of the tanks under consideration are much smaller than the critical value for convection. Therefore, convection in the settled solids layers is not expected.

References

Chandrasekhar S. 1981. *Hydrodynamic and Hydromagnetic Stability*. Dover Publications Inc., New York.

Katto Y and T Masuoka. 1967. "Criterion for the Onset of Convective Flow in a Fluid in a Porous Medium." *Int. J. Heat Mass Transfer*, Vol. 10, pp. 297-309.

McGrail BP, DS Trent, G Terrones, JD Hudson, and TE Michener. 1993. *Computational Analysis of Fluid Flow and Zonal Decomposition in Ferrocyanide Single-Shell Tanks*. PNL-8876, Pacific Northwest Laboratory, Richland, Washington.

Meyer PA, ME Brewster, SA Bryan, G Chen, LR Pederson, CW Stewart, and G Terrones. 1997. *Gas Retention and Release Behavior in Hanford Double-Shell Waste Tanks*. PNNL-11536 Rev. 1, Pacific Northwest National Laboratory, Richland, Washington.

Shekarriz A, DR Rector, LA Mahoney, MA Chieda, JM Bates, RE Bauer, NS Cannon, BE Hey, CG Linschooten, FJ Reitz, ER Siciliano. 1997. *Composition and Quantities of Retained Gas Measured in Hanford Waste Tanks 241-AW-101, A-101, AN-105, AN-104, and AN-103*. PNNL-11450 Rev. 1, Pacific Northwest National Laboratory, Richland, Washington.

Stewart CW, JM Alzheimer, ME Brewster, G Chen, RE Mendoza, HC Reid, CL Shepard, and G Terrones. 1996. *In Situ Rheology and Gas Volume in Hanford Double-Shell Waste Tanks*. PNNL-11296, Pacific Northwest National Laboratory, Richland, Washington.

Tveitereid M. 1977. "Thermal Convection in a Horizontal Porous Layer with Internal Heat Generation." *Int. J. Heat Mass Transfer*, Vol. 20, pp. 1045-1050.

Appendix C

Estimates of Ammonia Released by Convective Bubble Transport

Appendix C

Estimates of Ammonia Released by Convective Bubble Transport

The amount of ammonia being released into the tank headspace by convective transport in bubbles can be estimated by first calculating the total amount of gas being released into the headspace from the measured values of hydrogen in the headspace. This assumes that the only source of hydrogen in the headspace is from bubbles of retained gas. The total amount of gas released from bubbles can then be calculated using the fraction of retained gas that is due to hydrogen, which has been measured using the retained gas sampler (RGS) apparatus. Finally, the fraction of ammonia that is released by convective transport of bubbles can be calculated from the amount of gas in the headspace due to bubbles of retained gas and the fraction of ammonia in retained gas. The fraction of ammonia in the retained gas has also been measured using the RGS. The calculation has been performed for Tanks AW-101, AN-105, A-101, and U-103. It should be emphasized that this calculation only gives a rough, order-of-magnitude estimate of the amount of ammonia carried to the surface in bubbles. A rigorous error analysis has not been carried out on this calculation.

The concentration of hydrogen and ammonia in the headspace for the four tanks under consideration is given in Table C.1. The concentrations for Tanks AW-101 and AN-105 were obtained from Wilkins et al. (1997); the concentrations for Tanks A-101 and U-103 were obtained from the data summary of headspace measurements reported in Palmer et al. (1996). The conversion from mg/cm^3 to ppm for Tanks A-101 and U-103 assumes that the headspace is at standard conditions. This introduces a small error into the calculations but does not alter the conclusion.

The average mole fraction, f_{H2}, of hydrogen in the bubbles is calculated by averaging the values from Table 4.52 of Shekarriz et al. (1997) for Tanks AW-101, AN-105, and A-101. For Tank U-103, the value was obtained from a PNNL letter report .[(a)] The mole fraction of ammonia in the bubbles, f_{NH3}, of Tanks AW-101, AN-105, and A-101 was obtained from Table 4.53 of Shekarriz et al. (1997). The mole fraction of ammonia in the bubbles of Tank U-103 was obtained from the previously cited PNNL letter report. The values of the mole fractions are also included in Table C.1. Once this information was collected, the concentration of ammonia in the headspace from convective transport in bubbles was calculated using the relation

$$C_{NH_3} = C_{H_2} \frac{f_{NH_3}}{f_{NH_2}}$$

The values obtained for Tanks AW-101, AN-105, A-101, and U-103 are 0.08 ppm, 0.01 ppm, 32 ppm, and 46 ppm, respectively. These are all at least a factor of 10 smaller than the measured values of the ammonia concentration listed in Table C.1, indicating that convective transport of ammonia inside bubbles accounts for a fairly small fraction of the ammonia in the headspace.

(a) Mahoney LA, ZI Antoniak, JM Bates, and A Shekarriz. May 1997. *Preliminary Retained Gas Sampler Measurement Results for Hanford Waste Tank 241-U-103.* TWSFG97.40, Pacific Northwest Laboratory, Richland, Washington, Table 6.

Table C.1. Hydrogen and Ammonia Headspace Concentration

	AW-101	AN-105	A-101	U-103
H_2 (ppm)	37	27	638	493
NH_3 (ppm)	7	15	631	644
f_{H2}	0.271	0.427	0.478	0.26
f_{NH3}	0.0006	0.0002	0.024	0.02

References

Palmer BJ, CM Anderson, G Chen, JM Cuta, TA Ferryman, and G Terrones. 1996. *Evaluation of the Potential for Significant Ammonia Releases from Hanford Waste Tanks*. PNNL-11237, Pacific Northwest National Laboratory, Richland, Washington.

Shekarriz A, DR Rector, LA Mahoney, MA Chieda, JM Bates, RE Bauer, NS Cannon, BE Hey, CG Linschooten, FJ Reitz, ER Siciliano. 1997. *Composition and Quantities of Retained Gas Measured in Hanford Waste Tanks 241-AW-101, A-101, AN-105, AN-104, and AN-103*. PNNL-11450 Rev. 1, Pacific Northwest National Laboratory, Richland, Washington.

Wilkins NE, RE Bauer, and DM Ogden. 1997. *Results of Vapor Space Monitoring of Flammable Gas Watch List*. HNF-SD-WM-TI-797 Rev. 1, Lockheed Martin Hanford Corporation, Richland, Washington.

Appendix D

Monte Carlo Calculations of Uncertainty

Appendix D

Monte Carlo Calculations of Uncertainty

Monte Carlo simulations were carried out to calculate the distribution of effective diffusivities for a large number of randomly generated input parameters. Normal (Gaussian) distributions were used for most of the input parameters except for the ammonia concentrations in the waste and the Henry's law constants, for which uniform distributions were used. For the ammonia concentrations, the uniform distribution was used since it represents the uncertainty in the scaling factor; and for the Henry's law constants the uniform distribution was used because the Henry's law constants have large uncertainties in their determination that can cause them to vary by as much as a factor of nine in the DSTs. If nonphysical input values were generated for some of the parameters (i.e., negative values for positive quantities like the water mass fraction), the input was rejected and another generated. This resulted in a normal distribution that was truncated at zero.

The computed distributions for the diffusivities and the generation rate factor for AW-101 are shown in Figures D.1 through D.3. Distribution calculations in all tanks exhibit behavior similar to that of Tank AW-101, namely, approximately lognormal distributions for the diffusivities and normal distributions for the generation rates.

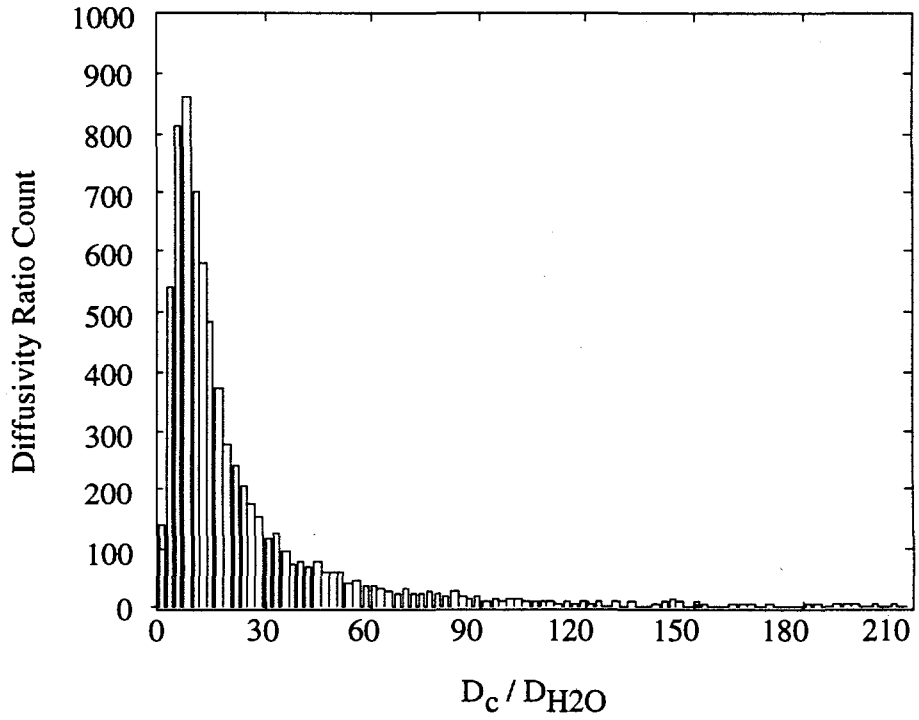

Figure D.1. Distribution of the Diffusivity Ratios for the Floating Solids Layer in Tank AW-101

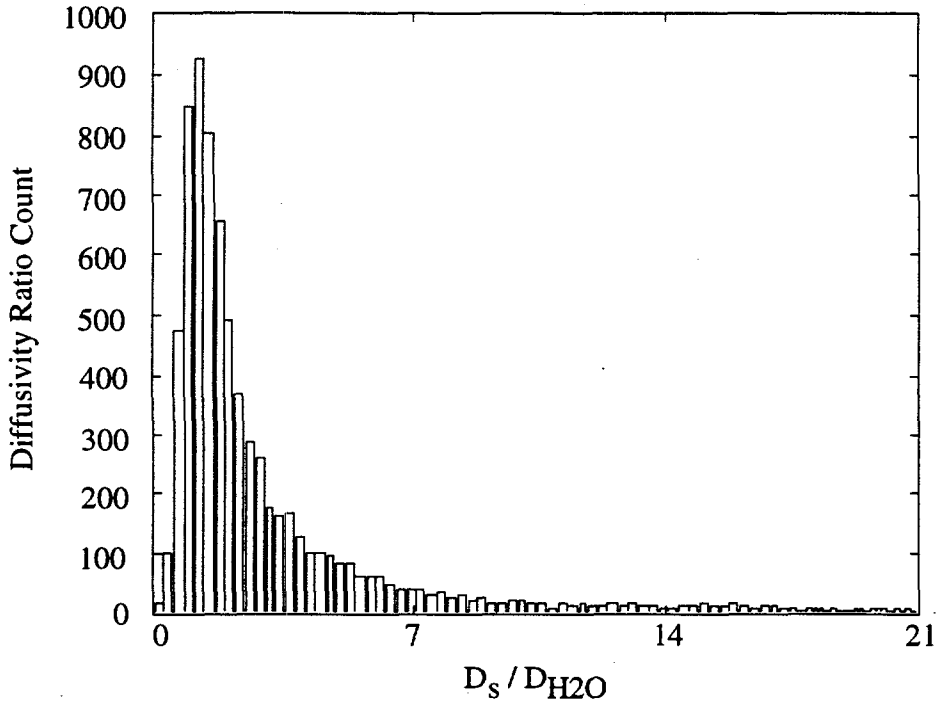

Figure D.2. Distribution of the Diffusivity Ratios for the Settled Solids Layer in Tank AW-101

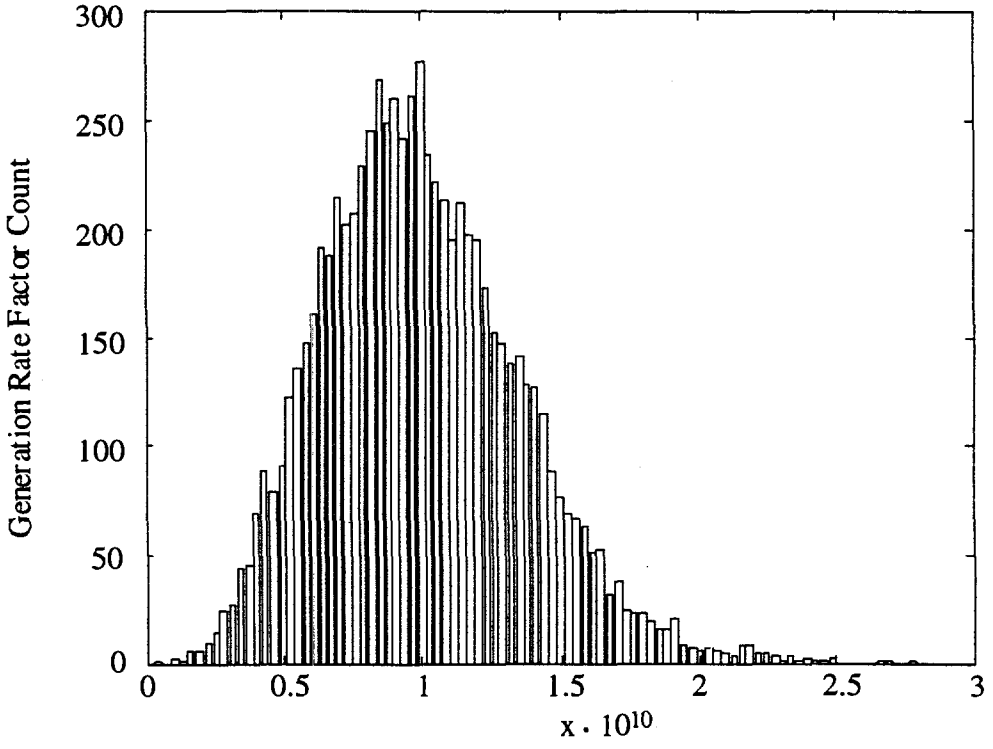

Figure D.3. Distribution of the Generation Rate Factor x in Tank AW-101

Appendix E

Numerical Solution of Ammonia Concentration Model for Double-Shell Tanks

Appendix E

Numerical Solution of Ammonia Concentration Model for Double-Shell Tanks

The NH_3 concentration model for double-shell tanks (DSTs) described in Section 2.1 of the main report can be solved by converting the concentration equations to finite-difference form. In this approach, the concentration at each axial level can be expressed as the matrix equation:

$$\overline{\overline{A}} \cdot \overline{C} = \overline{S}$$

In this formulation, $\overline{C}$ is a vector consisting of the ammonia concentration as a function of axial location in the tank, which includes a settled solids layer, a supernatant liquid layer, a floating solids layer, and the headspace under the tank dome. The settled solids and floating solids layers are each represented by a finite-difference axial nodes, the exact number of nodes specified by input. The supernatant liquid layer is represented by a single node, as is the headspace. The matrix $\overline{\overline{A}}$ is the tridiagonal coefficient matrix for the concentration vector, expressed in finite-difference form. The vector $\overline{S}$ represents the right side of the concentration equation for each level.

The equation set represented by this matrix equation can be solved using a Crank-Nicholson algorithm, by the simple expedient of inverting matrix $\overline{\overline{A}}$ and multiplying the result by matrix $\overline{S}$. Using a fully implicit formulation of the algorithm, there is no time-step size limitation for stability. The only criterion is the time-scale of significant changes in the ammonia concentration in the tanks. The time step must be small enough to capture the transient but large enough to allow efficient use of computer resources.

This numerical solution was implemented on a SUN Ultra-1 workstation, and calculations were performed with time steps of days, months, and years for a range of postulated tank configurations. It was determined that a time-step size on the order of a few months is sufficient to capture transient behavior in the tanks.

Using a time step of 0.1 year (1.2 months, or 36.5 days), calculations were performed to determine the transient concentrations for DSTs AW-101, AN-103, AN-104, and AN-105. Table E.1 gives the calculated concentrations in the headspace and supernatant liquid, average concentrations predicted for the settled solids and floating solids layers, plus the elapsed time required to approach the steady-state concentration values. The transient calculations show that a relatively long time is required for these tanks to reach steady state; 20 years is the shortest interval (for Tank AN-105), and the longest interval is approximately 76 years (for Tank AN-103). However, the concentrations are predicted to be within 30% of the steady-state values in a time interval that is only about a tenth as long as the time to steady state (i.e., 7.8 years for Tank AN-105 and 10.4 years for Tank AN-103). Also, the concentrations are within 5% of their steady-state values in approximately half the time it takes to reach steady state in a given tank. These results indicate that the concentration profiles approach their steady-state values on a long slow asymptote, with the largest changes in concentration occurring in the first few months or years of the transient.

Table E.1. Ammonia Concentration Calculations in Double-Shell Tanks

	AW-101	AN-103	AN-104	AN-105
C_a (μM)	0.45	0.30	0.38	1.15
Average C_c (μM)	239	243	300	212
C_l (μM)	871	1378	941	798
Average C_s (μM)	1770	1343	1746	1189
Time to steady-state converged to 99.99% (yr)	51	76	65.6	19.6
Time to bring C_a to within 30% of steady-state value (yr)	5.6	10.4	9.1	2.8
Time to bring C_a to within 20% of steady-state value (yr)	8.2	15.2	13.7	3.9
Time to bring C_a to within 10% of steady-state value (yr)	13.7	25	23.1	6.2
Time to bring C_a to within 5% of steady-state value (yr)	20.3	35.8	32.6	8.5

Distribution

No. of Copies

Offsite

2 DOE Office of Scientific and Technical Information

E. K. Barefield
Bogg Chemistry Building
Georgia Institute of Technology
225 North Avenue
Atlanta GA 30332

C. W. Forsberg
Oak Ridge National Laboratory
P.O. Box 2008, MS-6495
Oak Ridge, TN 37831-6495

B. C. Hudson
P.O. Box 271
Lindsborg, KS 67456

J. L. Kovach
P.O. Box 29151
70000 Huntley Road
Columbus, OH 43229

3 Los Alamos National Laboratory
P.O. Box 1663
Los Alamos, NM 87545
Attn: S. F. Agnew K575
W. L. Kubic K575
W. R. Bohl K575

D. A. Powers
Sandia National Laboratories
MS-0744
Albuquerque, NM 87185-0744

Onsite

5 DOE Richland Operations Office

K Chen	S7-54
C. A. Groendyke	S7-54
W. F. Hendrickson	S7-54
G. M. Neath	S7-51
G. W. Rosenwald	S7-54

No. of Copies

24 PHMC Team

G. S. Barney	T5-12
W. B. Barton	R2-12
R. E. Bauer	S7-14
D. R. Bratzel	S7-14
R. J. Cash	S7-14
D. L. Herting	T6-07
K. M. Hodgson	R2-11
J. R. Jewett	T6-07
G. D. Johnson (5)	S7-14
N. W. Kirch	R2-11
J. W. Lentsch	S2-48
J. E. Meacham	S7-14
J. C. Person	T6-07
D. A. Reynolds	R2-11
E. R. Siciliano	HO-31
L. M. Stock	S7-14
R. J. Van Vleet	A3-34

36 Pacific Northwest National Laboratory

Z. I. Antoniak	K7-15
J. M. Bates	K7-15
S. Q. Bennett	K7-90
J. W. Brothers (5)	K5-22
S. A. Bryan	P7-25
D. M. Camaioni	K2-44
J. M. Cuta	K7-15
T. A. Ferryman	K5-12
P. A. Gauglitz	P7-41
L. A. Mahoney	K7-15
P. A. Meyer	K7-15
B. J. Palmer (10)	K7-15
L. R. Pederson	K2-44
L. M. Peurrung	P7-41
S. D. Rassat	P7-41
C. W. Stewart	K7-15
G. Terrones	K7-15
Information Release (5)	K1-06